Title

Genetic and pharmacologic suppression of PPARγ enhances NELL-1-stimulated bone regeneration.

Authors

Tanjaya, Justine
Ha, Pin
Zhang, Yulong
et al.

Publication Date

2022-08-01

DOI

10.1016/j.biomaterials.2022.121609

HHS Public Access

Author manuscript

Biomaterials. Author manuscript; available in PMC 2023 October 23.

Published in final edited form as:

Biomaterials. 2022 August ; 287: 121609. doi:10.1016/j.biomaterials.2022.121609.

Genetic and pharmacologic suppression of PPARγ enhances NELL-1-stimulated bone regeneration

Justine Tanjaya[1], **Pin Ha**[1], **Yulong Zhang**[2], **Chenchao Wang**[1], **Yash Shah**[1], **Emily Berthiaume**[5], **Hsin Chuan Pan**[1], **Jiayu Shi**[1], **Jinny Kwak**[1], **Benjamin Wu**[2,#], **Kang Ting, D.M.D., D.MED.SC.**[3,#,*], **Xinli Zhang, M.D., Ph.D.**[1,#,*], **Chia Soo, M.D., F.A.C.S.**[4,5,#,*]

[1]Section of Orthodontics, Division of Growth and Development, School of Dentistry, University of California, Los Angeles, Los Angeles, California, USA, 90025

[2]Departments of Materials Science and Engineering and Division of Advanced Prosthodontics, University of California, Los Angeles, Los Angeles, California, USA, 90025

[3]Forsyth Institute, Harvard University, Cambridge, Massachusetts, USA, 02142

[4]Division of Plastic and Reconstructive Surgery and Department of Orthopaedic Surgery and the Orthopaedic Hospital Research Center, University of California, Los Angeles, Los Angeles, California, USA, 90025

[5]David Geffen School of Medicine, University of California, Los Angeles, Los Angeles, California, USA, 90025

Abstract

Recent investigations into mechanisms behind the development of osteoporosis suggest that suppressing PPARγ-mediated adipogenesis can improve bone formation and bone mineral density. In this study, we investigated a co-treatment strategy to enhance bone formation by combining NELL-1, an osteogenic molecule that has been extensively studied for its potential use as a therapeutic for osteoporosis, with two methods of PPARγ suppression. First, we suppressed PPARγ genetically using lentiviral PPARγ-shRNA in immunocompromised mice for a proof of concept. Second, we used a PPARγ antagonist to suppress PPARγ pharmacologically in immunocompetent senile osteopenic mice for clinical transability. We found that the co-treatment strategy significantly increased bone formation, increased the proliferation stage cell population,

[*]Correspondence should be addressed to Kang Ting (erickangting@gmail.com), Xinli Zhang (xzhang@dentistry.ucla.edu), and Chia Soo (bsoo@ucla.edu), Kang Ting, D.M.D., D.MED.SC., Forsyth Institute, Harvard University, 245 First Street, Cambridge, MA 02142, Xinli Zhang, M.D., Ph.D., Section of Orthodontics, School of Dentistry, University of California, Los Angeles, 675 Charles E. Young Dr. South, Rm 2641A, Los Angeles, CA 90025, Chia Soo, M.D., F.A.C.S., Division of Plastic and Reconstructive Surgery and Department of Orthopaedic Surgery and the Orthopaedic Hospital Research Center, University of California, Los Angeles, 675 Charles E. Young Dr. South, Rm 2641A, Los Angeles, CA 90025, Tel: 1-310-794-5479, Fax: 1-310-206-7783.

[#]Co-senior authors

AUTHOR CONTRIBUTIONS

Conceptualization, J.T., X.Z., and K.T.; Methodology, J.T. and X.Z.; Investigation, J.T., P.H., Y.Z., C.W., Y.S., H.S.P., and J.S.; Writing – Original Draft, J.T. and X.Z.; Writing – Review & Editing, J.T., E.B., X.Z., B.W., K.T., and C.S.; Funding Acquisition, X.Z., B.W., K.T., and C.S.; Resources, X.Z., J.K., B.W., K.T., and C.S.; Supervision, X.Z., B.W., K.T., and C.S.

Conflict of Interest Statement:

X.Z., B.W., K.T., and C.S. are inventors of NELL-1-related patents. X.Z., B.W., K.T., and C.S. are founders and/or board members of Bone Biologics Inc., which sublicenses NELL-1 patents from the UC Regents, and also hold equity in the company. C.T.C. is an inventor of NELL-1-related patents filed from Oak Ridge National Laboratory (ORNL) and is a founder of NellOne Therapeutics Inc., which licenses NELL-1-related patent applications from ORNL. The remaining authors declare no competing financial interests.

decreased late apoptosis of primary mouse BMSCs, and increased osteogenic marker mRNA levels in comparison to the single agent treatment groups. The addition of PPARγ suppression to NELL-1 therapy enhanced NELL-1's effects on bone formation by upregulating anabolic processes without altering NELL-1's inhibitory effects on osteoclastic and adipogenic activities. Our findings suggest that combining PPARγ suppression with therapeutic NELL-1 may be a viable method that can be further developed as a novel strategy to reverse bone loss and decrease marrow adiposity in age-related osteoporosis.

Keywords

PPARγ; NELL-1; adipogenesis; bone regeneration; bone mineralization

INTRODUCTION

As the master transcriptional regulator of adipogenesis, activation of peroxisome proliferator-activated receptor gamma (PPARγ)[1, 2] has been found to negatively affect osteoblastic and osteoclastic activities[3–5], lead to an accumulation of adipose tissue in bone marrow, and reduce bone formation[6–8]. In agreement with these observations, our previous study found that intramedullary delivery of lentiviral PPARγ-shRNA significantly suppressed the formation of bone marrow adipose tissue, and instead, increased femoral epiphyseal trabecular bone volume[9]. With these encouraging results, we explored the potential of combining PPARγ suppression treatment with an osteoinductive molecule to enhance bone augmentation and suppress bone marrow adipose formation. However, we found that using bone morphogenetic protein-2 (BMP2) while simultaneously inhibiting PPARγ did not improve BMP2-induced bone regeneration, and even appeared to prevent bony union in large femoral segmental defects[10]. The varying results of PPARγ inhibition on osteogenesis may suggest that additional factors, such as PPARγ cellular signaling pathways or cellular microenvironments, particularly when used in a combinatorial treatment setting, may play crucial roles in determining the fate of osteogenic induction with concomitant adipogenic suppression. Therefore, further studies are required to investigate the use of combinatorial treatments that may induce osteogenesis and suppress adipogenesis for improved bone regeneration. One area of investigation may be into the activity of Wnt, a multifaceted regulator. The Wnt pathway governs a substantial amount of bone remodeling and resorption activities[11, 12]. Reduced Wnt signaling activity has been found to result in osteoporotic features, while increased Wnt signaling, via inactivation of endogenous Wnt inhibitors, promotes osteoblastic activities and bone formation[12–15]. Several studies have reported that Wnt pathway inhibition also promotes adipogenic programming at the expense of osteogenesis[6, 8]. It appears that regulating the balance between the Wnt/β-catenin and PPARγ signaling pathways through combinatorial treatment may be the key to improving bone regeneration and holds significant potential in combating osteoporosis in the clinical setting.

For the past two decades, NELL-1 has been studied extensively in various animal models for its use in bone repair and osteogenesis[9, 16–49]. NELL-1 has shown promising therapeutic potential in the bone engineering field, specifically in craniofacial and maxillofacial bone

regeneration[47, 50, 51], long bone segmental defect bone repair[32, 41, 52, 53], spinal fusion[24, 47, 54], and cartilage repair[40]. In 2014, our team successfully engineered the novel PEGylated NELL-1 (NELL-PEG) protein with prolonged osteogenic effects and longer half-life upon systemic delivery[49]. Since then, NELL-PEG has been continuously pursued as a potent systemic therapy for osteoporotic bone loss in challenging animal models including OVX-induced osteoporotic mice[27] and mice subjected to microgravity-induced severe systemic bone loss (unpublished data). As an osteogenic molecule that mechanistically differs from BMP2[20, 55], NELL-1 has exhibited considerable effects on both the PPARγ and Wnt/β-catenin signaling pathways[20, 21, 55]. As such, NELL-1 may hold the potential for modulating the PPARγ and Wnt/β-catenin signaling pathways during osteogenesis and/or adipogenesis.

A high-affinity ligand-receptor binding interaction between NELL-1 and cell surface receptor contactin-associated protein-like 4 (Cntnap4)/integrin α3β1 has previously been found on the surface of osteogenic lineage cells[29]. Upon binding, NELL-1 can activate the canonical Wnt/B-catenin[29], MAPK/JNK[29, 45], and/or Hedgehog (HH) signaling pathways[29]. These pathways lead to the activation of osteogenic transcription factors, increase bone anabolism, and suppress bone resorption[9, 16–49]. Additionally, NELL-1 has been found to reduce adipogenic differentiation in a human preadipocyte cell line and human adipose-derived stromal cells[9], which contrasts with FDA-approved BMP2 that has been found to create bone filled with adipocyte infiltrates[55–57]. To test the efficacy of NELL-1's anti-adipogenic effect, our team showed that the combination of NELL-1 and high-dose BMP2 significantly optimized osteogenesis by minimizing the formation of adipose-filled cyst-like bone[55, 57]. Even though our previous results showed some potential for NELL-1 to reduce adipogenesis, the role of PPARγ signaling pathways in mediating NELL-1-induced osteogenesis remains unknown. In this study, we aimed to discover the *in vivo* effects of genetic and pharmacologic PPARγ suppression when combined with NELL-1 and to investigate the underlying pathways involved in governing cellular bone remodeling processes. Ultimately, knowledge from this study may be used as a foundation to formulate a combination of PPARγ suppression with currently available anti-osteoporotic therapeutics to improve their efficacy and safety profiles in stimulating bone regeneration.

MATERIALS AND METHODS

B1. Animal models and intramedullary injection procedure.

Animals were housed in a 12-hour light cycle environment with *ad libitum* access to food and water. All animal procedures were conducted in accordance with the Guide for the Care and Use of Laboratory Animals of the University of California, Los Angeles and were approved by the Animal Research Committee (ARC).

Male severe combined immunodeficiency (SCID) mice (8 weeks old, n=5 per group) were obtained from Charles River Laboratories (Wilmington, MA) and kept under pathogen-free conditions with *ad libitum* access sterile food and acidified water. The animals were randomly assigned to the phosphate-buffered saline (PBS), PEGylated NELL-1[27, 49] (NELL-PEG, 600 ng/ml) (Aragen Bioscience), PPARγ-shRNA lentivirus (srPPARγ, 5×10^7

$TCID_{50}$/mL, MOI=10) (Santa Cruz Biotechnology), or co-treatment NELL-PEG + srPPARγ (NELL-PEG, 600 ng/mL and srPPARγ, 5×10^7 $TCID_{50}$/mL, MOI=10) treatment groups. Briefly, a 5 mm-longitudinal incision was made at the medial aspect of the quadriceps muscle to expose the patella. A 26-gauge needle was inserted through the defect. Ten microliters of the assigned treatment were injected into the intramedullary cavity of the bilateral femurs. The quadriceps–patellar complex was then repositioned and sutured closed with 5–0 Vicryl thread.

Female BALB/c mice (45 weeks old, n=5 per group) were obtained from Taconic Biosciences (Cambridge City, IN) and housed according to the standard operating procedure approved by the ARC protocol. The animals were randomly assigned to the PBS, NELL-PEG (600 ng/ml), bisphenol A diglycidyl ether (BADGE) (68 mg/ml, Cat. 1326; Bio-Techne Corporation)[58], or co-treatment NELL-PEG + BADGE treatment groups. All animals underwent the surgical procedure detailed for the male SCID mice.

B2. Viral production and purification.

The PPARγ-shRNA lentiviral vectors were generated by co-transfecting 293T cells with the PPARγ-shRNA plasmid vector (SC-29455-SH; Santa Cruz Biotechnology) or the FG12 vector (14884; Addgene) with the helper plasmids pCMV-dR8.2-vprX and pCMV-VSVG, respectively. The vectors were obtained by filtering to remove cellular debris and concentrated by ultracentrifuge at 4°C, 17,000 rpm for 60 min. The pellets containing the vectors were re-suspended with cell medium to a concentration of 5×10^7 $TCID_{50}$/mL. The lentiviral vector titer was determined by measuring the gag p24 protein. 1 pg of p24 was assigned as the 10 tissue culture infective dosage ($TCID_{50}$) for freshly isolated lentiviral vectors. Briefly, cells were plated at 30–50% confluence and transfected with appropriate dilutions of lentiviral particles (multiplicity of infection (MOI) = 10) for 24 h. A puromycin (sc-108071, Santa Cruz Biotechnology) titration (kill curve) was performed to optimize the concentration of puromycin. Cells were then cultured in growth medium containing 0.5 μg/mL puromycin to obtain stable transfected cell lines[59].

B3. Dual x-ray absorptiometry (DXA) analysis.

All animals underwent dual x-ray absorptiometry scanning (PIXImus2 GE Lunar Corp., Madison, WI) to monitor changes in BMD (g/cm^2). A square 10×10 mm^2 region of interest was marked at the distal femur. A longitudinal assessment of relative BMD change was performed by measuring BMD at baseline, before surgical procedures were performed, and post-surgically at 2 week intervals until the study endpoint[60].

B4. Microcomputed tomography (microCT) analysis.

MicroCT analysis was performed using the protocol detailed in a previous study[60]. Briefly, femur samples were harvested 8 weeks after intramedullary injection. Samples were fixed in formalin (4% PFA) and immersed in 70% ethanol. High-resolution microcomputed tomography (microCT; Skyscan 1176) scanning was performed with a resolution of 10 μm (55 kV, 181 mA, and 0.5 mm aluminum filter). For trabecular bone analysis, the region of interest (ROI) was located 1 mm away from the growth plate and drawn to select only metaphyseal intramedullary trabecular bone. To determine cortical bone density and

thickness, ROIs were drawn at the midshaft of the femoral diaphysis and the distal shaft of the femoral metaphysis. Trabecular and cortical bone parameters were analyzed using CTAn software version 1.13 (Bruker microCT N.V.) with a threshold value of 60 and 100, respectively. CTVox software version 3.3 (Bruker microCT N.V.) was used to generate three-dimensional (3D) representative images.

B5. Histological analysis.

Histological analysis was performed using the protocol from previous studies [25]. Femoral tissue was harvested after sacrifice, fixed in formalin (4% PFA), and decalcified using 19% ethylenediaminetetraacetic acid (EDTA) for a minimum of two weeks. The decalcified samples were cut along the coronal plane into 5-μm thick paraffin sections. All samples were analyzed under the microscope, and four consecutive images at the femoral midshaft and distal shaft were captured using CellSense software version 1.12 (Olympus Corp., Tokyo, Japan). All histomorphometric analyses of stained sections were performed in triplicate using ImageJ software.

B6. Immunohistochemical analysis.

Immunohistochemistry analysis was performed using the protocol detailed in a previous study[25]. Unstained sections were deparaffinized and incubated with primary anti-OCN (1:100, Santa Cruz), anti-PPARγ (1:200, Santa Cruz), and anti-β-catenin (1:1000, Abcam) antibodies. The sections were then incubated by the corresponding biotinylated secondary antibodies (1:200–1000) (Dako). Positive expression was detected using avidin-biotin complex (ABC) (PK-6100, Vectastain Elite ABC Kit; Vector Laboratories, Inc.) incubation and development with amino ethyl carbazole (AEC) chromogen (K346911–2; Dako). Sections were counterstained with hematoxylin for 10 seconds and then rinsed with water. Photomicrographs were acquired using Keyence BZ-X700 (Japan). TRAP staining was performed according to the manufacturer's protocol (Procedure No. 387, Sigma-Aldrich). For the OCN and TRAP staining, the number of positively stained osteoblasts present along the bone perimeter were determined by three blinded observers. For the PPARγ and β-catenin staining, staining intensity was analyzed using ImageJ software and is presented as relative staining area divided by total cell area. Results are presented as an average of six random fields for each sample.

B7. Cell culture.

Cells from an immortalized mouse bone marrow-derived stem cell (BMSC) cell line, M2–10B4 (M2) (ATCC, Manassas, VA), were used and maintained in Roswell Park Memorial Institute (RPMI) 1640 growth medium (Invitrogen, Carlsbad, CA) with the addition of 10% fetal bovine serum (FBS), 1 mmol/L sodium pyruvate, and 100 U/mL penicillin/streptomycin (Gibco). All cells were plated into 6-well plastic cell culture plates at a density of 5×10^5 cells per well. Osteogenic differentiation was induced for 21 days with RPMI 1640 medium, 10% fetal bovine serum, 50 mg/mL ascorbic acid, and 3 mmol/L b-glycerophosphate. Adipogenic differentiation was induced for 21 days in AdipoMAX differentiation medium (SCM122–1KT, Sigma) with the addition of a 10 mL dilution factor component (SCM122–1KT, Sigma). The culture medium was exchanged every 3 days. The selected clonal stable PPARγ knockdown M2 cells (M2-PP) and scramble control (M2-SC)

cells were also cultured and differentiated in an analogous manner to their parental M2 cells[10].

Freshly isolated BMSCs were collected from 45-week-old female BALB/c mouse femurs (n=3 per group). Femurs were dissected, and bone marrow was flushed using a syringe needle containing Dulbecco's Modified Eagle Medium (DMEM) (Gibco). The collected BMSCs were filtered through a 70-mm nylon mesh filter (BD, Falcon) to remove unwanted debris. All cells were plated into 12-well plastic cell culture plates at a density of 5×10^5 cells per well in 50 mL DMEM growth medium containing 15% fetal bovine serum (FBS; Sigma-Aldrich), 2 mm L-glutamine (Gibco BRL), and 100 U/mL penicillin (Gibco). Cultures were kept at 37°C in a humidified incubator with a 95% air and 5% CO_2 atmospheric environment.

B8. Mineralization assay.

The M2 cells were cultured with osteogenic medium for 21 days, with the medium being exchanged every 3 days. At day 21, the cells were stained with Alizarin Red according to the manufacturer's protocol (CM-0058; Lifeline Cell Technology, Frederick, MD) and then rinsed with PBS. Briefly, monolayers were fixed with 3 mL absolute ethanol per well for 30 minutes at room temperature and then rinsed with PBS. Cells were then stained with Alizarin Red Stain Solution (CM-0058; Lifeline Cell Technology, Frederick, MD) for 15 minutes and then rinsed with PBS. The intensity of staining was analyzed using ImageJ software and is presented as relative staining area divided by total cell area[61].

B9. Adipocyte differentiation assay.

The M2, M2-PP, and M2-SC cells were cultured with adipogenic medium for 21 days, with the medium being exchanged every 3 days. All cells were plated into 12-well plastic cell culture plates at a density of 5×10^5 cells per well. At day 21, Oil Red O staining was performed according to the manufacturer's protocol (LL-052, Lifeline Cell Technology). Monolayers were rinsed with PBS, fixed with 4% PFA for 60 min at room temperature, and dehydrated using 1,2-Propanediol Dehydration Solution (CM-0056, Lifeline Cell Technology). Cells were stained with 2 mL of Oil Red O solution (CM-0054, Lifeline Cell Technology) at 37°C for 30 min. The intensity of staining was analyzed using ImageJ software and is presented as relative staining area divided by total cell area.

B10. Flow cytometry analysis for cell proliferation and apoptosis assays.

To analyze cell proliferation, M2 and M2-PP cells were treated either with PBS or NELL-1 (300 ng/mL) for 3 days and then subjected to flow cytometry using the FITC BrdU Flow Kit (Cat. 559619, BD Pharmingen). Cells were stained with 7-Aminoactinomycin D (7-AAD) and analyzed according to the manufacturer's instructions. To analyze cell apoptosis, M2 and M2-PP cells were treated with either PBS or NELL-1 (300 ng/mL) for 3 days and subjected to flow cytometry using the FITC Annexin V/Dead Cell Apoptosis Kit protocol (Cat. 556547, BD Biosciences). Freshly isolated BMSCs were obtained from 45-week-old female BALB/c mice on day 0 without any injection (baseline), and day 3 and 7 after intramedullary injection. Animals were injected with intraperitoneal (IP) BrdU solution (10 mg/mL) 3 hours before sacrifice. Harvested cells were subjected to fluorescence-activated

cell sorting (FACS) analysis for cell proliferation and cell apoptosis assays. All results were analyzed with FACS Diva software version 4.0 (BD Biosciences).

B11. Real-time polymerase chain reaction analysis.

Total RNA for real-time polymerase chain reaction (RT-PCR) evaluation was extracted from the M2 and M2-PP cells using TRIzol reagent (Invitrogen) at days 0, 3, 6, and 9, respectively. For freshly isolated BMSCs, the total RNA was collected at days 0, 3, and 7 post-injection. After isopropyl alcohol precipitation, the total RNA was treated with ezDNase enzyme and 10x ezDNase buffer according to the manufacturer's protocol (Cat. 11766050, Thermo Fisher Scientific) to initiate the reverse transcription process. cDNA was then mixed with SuperScript IV VILO Master Mix (Invitrogen) and nuclease-free water for a final volume of 20 μL. Real-time PCR reactions were performed in triplicate in 96-well plates using the 7300 Real-Time PCR System (Applied Biosystems) in which the DNA was subjected to 95°C for 10 min, followed by 40 cycles at 95°C for 15 s, and cooling at 60°C for 10 s. The Ct was defined as the fractional cycle number at which the fluorescence passes the fixed threshold. The respective pairs of primer sequences of mouse PPARγ2 were sense: ATGCACTGCCTATGAGCACT and anti-sense: CAACTGTGGTAAAGGGCTTG; mouse RUNX2 were sense: CGGTCTCCTTCCAGGATGGT and anti-sense: GCTTCCGTCAGCGTCAACA; mouse OCN were sense: GGGAGACAACAGGGAGGAAAC and anti-sense: CAGGCTTCCTGCCAGTACCT; mouse CEBPα were sense: TGAACAAGAACAGCAACGAG and antisense: TCACTGGTCACCTCCAGCAC; mouse Ki67 were sense: GATGGAAGCATTGTGAGAACCA and antisense: CCTGCTCTTCCACAGATTCAAG; and mouse GADPH were sense: TGCACCACCAACTGCTTAGC and anti-sense: CCACCACCCTGTTGCTGTAG. The relative expression levels were compared to glyceraldehyde 3-phosphate dehydrogenase (GAPDH).

B12. Statistical analysis.

Standard descriptive statistics and 95% confidence intervals (CI)s were estimated, and data were assessed for normal distributions. Data were analyzed with one way ANOVA when multiple groups were compared with each other. For longitudinal measurements, percentage of change over time was modeled using a linear mixed model and nonparametric analysis of the mean BMD of each treatment group was compared with the mean of the PBS control at each time point. All analyses were performed using the GraphPad Prism software v 7.0 (San Diego, CA). Data are expressed as means ± SD except for the DXA data, for which the findings are expressed as the means ± SEM. Statistical significance was selected at $*p<0.05$ and $**p<0.01$.

RESULTS

Suppression of PPARγ via intramedullary lentiviral shRNA (srPPARγ) injection promoted bone formation in young SCID mice and additively enhanced PEGylated NELL-1's (NELL-PEG's) osteogenic effects.

In relation to our previous work investigating the effects of PPARγ inhibition on bone formation[59] when used in combination with BMP2[10], we first utilized lentiviral srPPARγ intramedullary injections in a young SCID mouse model as a 'proof-of-principle'. At 8 weeks post-injection, high-resolution microCT analysis at the distal shaft (DS) of the femoral metaphysis showed the highest relative increase in bone mineral density (BMD) and trabecular bone formation in animals that underwent co-treatment with srPPARγ + NELL-PEG (Figure 1A–E). Co-treatment with PPARγ suppression + NELL-PEG additively increased these parameters compared to the single agent srPPARγ or NELL-PEG treatment groups. No significant difference was found among the single agent treatment groups (Figure 1D–E). Compared to the PBS group, the BMD and bone volume/total volume (BV/TV) of the srPPARγ + NELL-PEG group were significantly increased by almost two-fold (Figure 1D–E). MicroCT quantification of cortical bone at the midshaft (MS) of the femoral diaphysis showed a significant increase in tissue mineral density (TMD) and cortical thickness in the co-treatment group compared to the PBS or srPPARγ groups (Figure 1F–G). When comparing the co-treatment group to the NELL-PEG group, a statistically significant difference was found for cortical TMD at the MS (Figure 1F). MicroCT quantification of cortical bone at the DS of the femoral metaphysis showed a significant increase in tissue mineral density (TMD) in the srPPARγ + NELL-PEG group compared to the PBS or srPPARγ groups (Figure 1H). The cortical thickness in co-treatment group was significantly increased compared to all of the other groups (Figure 1I). Longitudinal DXA BMD was significantly increased in both the single agent srPPARγ and NELL-PEG treatment groups compared to the PBS group at weeks 2 and 4. The co-treatment group showed the highest BMD, which was significant compared to the PBS control at weeks 2, 4, 6, and 8 (Figure 1J). Histological evaluation (Figure 1K) and immunohistochemical staining of an osteogenic marker, osteocalcin (OCN) (Figure 1L), showed a significant increase in trabecular bone formation in all treatment groups compared to the PBS control. Specifically, the co-treatment group had a substantial increase in OCN-positive cells, by 140% and 48%, compared to the single agent srPPARγ and NELL-PEG groups, respectively (Figure 1M).

Suppression of PPARγ using a synthetic antagonist promoted bone formation in immunocompetent senile mice and additively enhanced NELL-PEG-induced osteogenesis to improve osteopenia.

We recapitulated the previously described experiment using a clinically relevant model, 45 week old immunocompetent senile BALB/c mice[62], to mimic age-related human osteopenia with the addition of a PPARγ antagonist, BADGE (Figure 2A–C). There was a marked increase in BMD and BV/TV in all treatment groups tested, including the BADGE, NELL-PEG, and BADGE + NELL-PEG groups. In particular, the BADGE + NELL-PEG group had significantly increased BMD and BV/TV in comparison to the PBS control, BADGE, and NELL-PEG treatment groups (Figure 2D–E). The TMD analysis revealed a similar trend with significantly enhanced cortical TMD and thickness in the

co-treatment group compared to the PBS control or BADGE treatment groups (Figure 2F–I). No statistical significance was observed for the cortical TMD analysis at the MS for the BADGE + NELL-PEG group in comparison to the NELL-PEG group (Figure 2F). No significant difference was found for the TMD analysis at the DS in the co-treatment group compared to the single agent BADGE or NELL-PEG treatment groups; however, these parameters were relatively increased in the co-treatment group (Figure 2H). The cortical thickness at the DS was significantly increased in the co-treatment group compared to the BADGE treatment group (Figure 2I). DXA BMD analysis showed a relative increase in all groups treated with therapeutic agents, whereas the PBS control group's BMD decreased over time (Figure 2J). The BADGE + NELL-PEG and NELL-PEG groups had a significantly increased BMD in comparison to the BADGE group at weeks 2, 4, 6, and 8. When compared to the PBS group, the increase in BMD of the BADGE group was significant at week 4 of treatment. Overall, the PBS group's BMD appeared to plateau starting at week 4 until the end of the study, whereas the co-treatment group had maintained a high BMD until the end of study (Figure 2J). Histology (Figure 2K) and immunohistochemistry (Figure 2L) analyses showed increased osteoblastic activity in all of the treatment groups, which significantly improved osteogenesis at the distal femoral metaphysis. Using the co-treatment of BADGE + NELL-PEG resulted in osteoblastic activity improvements of 91.5% and 77.5% compared to the single agent NELL-PEG or BADGE groups, respectively (Figure 2M).

Lentiviral PPARγ suppression did not augment NELL-PEG's inhibitory effects on adipose marrow formation and bone resorption in SCID mice.

Hematoxylin & eosin staining (H&E) (Figure 3A) and immunohistochemistry analyses at the femoral MS showed an increase in bone marrow adipocyte formation in the young SCID mouse PBS-treated group. Additionally, histochemical expression of PPARγ was significantly increased in the PBS control group (Figure 3B–C). The single agent srPPARγ knockdown and NELL-PEG treatment groups showed minimal adipocyte infiltration and PPARγ positive staining. Similarly, the srPPARγ + NELL-PEG group had decreased adipose marrow formation; however, the co-treatment did not appear to augment these effects when compared with single srPPARγ or NELL-PEG treatment alone. Accordingly, the histochemical analysis of PPARγ staining showed no significant difference among the srPPARγ, NELL-PEG, and the srPPARγ + NELL-PEG groups (Figure 3B–C). Immunostaining revealed an appreciably higher expression of β-catenin in the NELL-PEG + srPPARγ group compared to the srPPARγ or PBS groups (Figure S1A–B). Tartrate resistant acid phosphatase (TRAP) staining demonstrated significantly decreased osteoclast cell presence in the srPPARγ, NELL-PEG, and co-treatment groups compared to the PBS group (Figure 3D–E). TRAP staining analysis revealed fewer osteoclasts in the co-treatment group than in the srPPARγ group, and the fewest number of osteoclasts were found in the NELL-PEG group (Figure 3D–E).

PPARγ antagonism did not enhance NELL-PEG's inhibitory effects on adipose marrow formation and bone resorption in senile osteopenic mice.

Using an osteopenic mouse model and H&E staining, we observed that adipose tissue formation in the bone marrow was significantly suppressed in all treatment groups

(Figure 4A). However, we also observed variation among samples from the PBS group; three samples had higher fatty marrow formation, whereas the remaining samples had a similar amount of adipose marrow formation compared to the BADGE, NELL-PEG, and co-treatment group samples (Figure 4A). From the immunohistochemical PPARγ staining analysis, the BADGE, NELL-PEG, and co-treatment groups had decreased PPARγ staining in comparison to the PBS group; no statistically significant differences were found between these treatment groups (Figure 4B–C). Similar to the findings in the SCID mice, immunostaining revealed an appreciably higher expression of β-catenin in the NELL-PEG + BADGE group compared to the BADGE or PBS groups (Figure S2A–B). TRAP immunohistochemistry analysis demonstrated that the BADGE, NELL-PEG, and BADGE + NELL-PEG groups had significantly reduced osteoclastic activities at the distal femoral metaphysis in comparison to the PBS group (Figure 4D–E). The co-treatment group had fewer osteoclasts compared to srPPARγ group, but more osteoclasts than the NELL-PEG group. (Figure 4D–E).

Dual BADGE and NELL-PEG treatment significantly increased mineralization of primary BMSCs obtained from senile mice.

Primary BMSCs isolated from the mouse femurs 3 days post-injection were cultured in 12-well plates and incubated with a growth medium for 3 days. Alizarin Red staining analysis demonstrated that both the single agent BADGE and NELL-PEG-treated groups had increased mineralization capacities (Figure 5A). Co-treatment with BADGE + NELL-PEG significantly increased the BMSC osteogenic capacity by approximately 50% compared to cells cultured from the PBS-treated limbs. BMSCs obtained 7 days post-injection were collected and treated for the same incubation period. The results revealed significantly more abundant calcium-rich deposits in the NELL-PEG + BADGE group than the single agent NELL-PEG or BADGE treatment groups. In contrast, the PBS-treated group samples only had a few mineralized calcium formations (Figure 5A–B). These results suggest that treatment with NELL-1 could effectively suppress adipogenic differentiation when compared to the PBS treatment, and in addition, enhance BMSC mineralization when combined with BADGE.

The RT-PCR analysis revealed that co-treatment with NELL-PEG + BADGE significantly increased OCN and RUNX2 expression levels compared to the BADGE, NELL-PEG, and PBS groups (Figure 5C–D). The expression levels of PPARγ and CEBP/α were also evaluated using RT-PCR analysis. The NELL-PEG treatment group had significantly decreased PPARγ and CEBP/α mRNA expression levels, similar to the levels of the BADGE treatment group (Figure 5E–F). Co-treatment with NELL-PEG + BADGE did not have significantly different expression levels from the single agent NELL-PEG or BADGE treatment groups (Figure 5E–F), which coincides with the PPARγ histochemical findings reported in Figure 4B–C. Overall, these results suggest that PPARγ suppression with NELL-PEG + BADGE could significantly enhance osteogenic markers without altering adipogenic expression compared to using NELL-PEG or BADGE alone.

Dual BADGE and NELL-1 treatment significantly increased osteogenic gene expressions involved in the Wnt/β-catenin signaling pathway.

Using M2 cells, we examined the effects of dual BADGE and NELL-1 treatment on the components of the Wnt/β-catenin and PPARy signaling pathways. Our RT-PCR results suggested that, upon osteogenic stimulation, the combination treatment of NELL-1 application and PPARγ suppression showed increased β-catenin, GSK3b, Axin2, and OPG expressions (Figure S4A–F). We also found a similar trend when using freshly isolated BMSCs that were incubated with osteogenic differentiation medium for 3 days (Figure 6A–F). RANKL is expressed in BMSCs, but is not expressed in M2 cells. Upon osteogenic differentiation of BMSCs, RANKL was slightly increased in the NELL-1, BADGE, and dual BADGE + NELL-1 treated groups compared to the PBS control group (Figure 6G). Conversely, upon adipogenic differentiation of the BMSCs and M2 cells, the β-catenin, GSK3b, and OPG expressions were decreased (Figure 6H–N and Figure S4G–L).

NELL-1 exhibited a dose-dependent anti-adipogenic effect and the addition of srPPARγ treatment further enhanced NELL-1-induced osteogenesis, but not the anti-adipogenic effect.

While NELL-1's osteogenic effects have been previously described, the anti-adipogenic effect of NELL-1 has not been fully explored. We examined the anti-adipogenic effect using murine bone stromal M2 cells exposed to concentrations of NELL-1 ranging from 100–600 ng/mL (Figure S3A). Treatment with a low dose of NELL-1 (100 ng/mL) showed drastic adipogenic suppression compared to the PBS treatment (Figure S3A–B). Treatment with 300 ng/mL of NELL-1 appears to exert the maximum suppression of adipogenic differentiation detected by Oil Red O staining. As such, the dose-dependent anti-adipogenic effect of NELL-1 is likely present at doses less than 300ng/ml, which is the concentration at which the anti-adipogenic effect plateaued. Increasing the dose above 300 ng/mL did not significantly improve the anti-adipogenic potency of NELL-1 (Figure S3A–B). Although our previous studies indicate that NELL-1 exerts osteogenic effects in a dose-dependent manner, this effect seems to be neutralized when NELL-1 is combined with PPARγ suppression (Figure S3C–D).

We then explored how PPARγ suppression influenced NELL-1's anti-adipogenic effect. Suppressing PPARγ alone (srPPARγ) resulted in decreased adipogenesis compared to the scrambled control (srSC) group (Figure S3E). The addition of NELL-1 to the srPPARγ or srSC cells did not further reduce adipogenesis (Figure S3E–F). The RT-PCR analysis of the PPARγ and CEBP/α gene expression levels revealed that all treatment groups had significantly decreased mRNA expression levels compared to the PBS group. There were no significant differences found among the srPPARγ, NELL-1, and combination treatment groups. (Figure S3G–H).

We also tested the mineralization capacity of different treatments using M2–10B4 cells. The results showed that srPPARγ treatment alone enhanced mineralization compared to the PBS control. Furthermore, NELL-1 had a significantly enhanced osteogenic effect on srPPARγ cells, surpassing its osteogenic effect on srSC cells. (Figure S3H). Adding NELL-1 to the srPPARγ cells significantly enhanced mineralization by approximately two-fold compared

to the NELL-1 or srPPARγ treatments alone (Figure S3I). Staining with osteogenic markers OCN and RUNX2 supported findings from the Alizarin Red experiments with significantly increased osteogenic mRNA levels after co-treatment with NELL-1 + srPPARγ compared to all of the other tested treatments at all measured time points (Figure S3J–K).

BMSCs co-treated with BADGE + NELL-PEG had enhanced cell proliferation and attenuated apoptosis.

In all treatment groups, the PBS, NELL-PEG, BADGE, and BADGE + NELL-PEG groups, there was an increased percentage of freshly isolated BMSCs in S phase at day 3 and 7 post-injection compared to baseline (day 0 without any treatment), whereas the percentage of cells in the G0/G1 and G2/M phases was decreased (Figure 6A–C). At day 3, the NELL-PEG + BADGE treatment group had a significantly higher cell population in S phase compared to the PBS, NELL-PEG, and BADGE treatment groups (Figure 6A–B). In accordance, the percentage of cells in the G0/G1 and G2/M phases was decreased for the NELL-PEG and co-treatment groups. The BADGE treatment group had a significantly decreased percentage of cells in the G0/G1 phase, but had an increased percentage of cells in the G2/M phase compared to the other groups (Figure 6A–B). At day 7, the increased percentage of cells in S phase was significantly more prominent in the co-treatment group, with corresponding trends of decreased cell percentages in the G0/G1 and G2/M phases (Figure 6A–B). The Ki67 mRNA expression level was also significantly increased in the co-treatment group at day 3 and 7 compared to the PBS, NELL-PEG, and BADGE groups (Figure 6C), which corresponds to the flow cytometry cell cycle analysis findings.

Flow cytometry apoptosis analysis of fresh bone marrow cells cultured 3 days post-injection with NELL-PEG, BADGE, and co-treatment showed significantly decreased cell populations in the early and late apoptotic quadrants compared to the PBS group (Figure 7A–B). The NELL-PEG + BADGE treatment did not significantly decrease the percentage of apoptotic cells in the early apoptotic quadrant, but significantly decreased late apoptosis compared to the single agent NELL-PEG or BADGE treatment groups (Figure 7A–C). Similarly, there were no significant differences in the percentage of early apoptotic cells among the treatment groups on day 7; however, the NELL-PEG + BADGE treatment significantly attenuated the late apoptotic cell population percentage compared to the BADGE treated cells (Figure 7A–C). The apoptotic effect was also evaluated using murine bone marrow cell line M2–10B4 cells. Briefly, cells were incubated in an osteogenic medium mixed with BrdU for 3 days. Flow cytometry cell cycle analysis showed that knocking down PPARγ alone via srPPARγ slightly increased cell proliferation, which approached cell proliferation activity found in the NELL-1 treatment group (Figure S4A). Adding NELL-1 to the PPARγ knockdown cells significantly increased the percentage of cells in S phase compared to treatment with NELL-1 or srPPARγ alone (Figure S4B). The lentiviral scramble PBS treatment had significantly lower G0/G1 and G2 cell populations compared to the PBS control group. Additionally, the lentiviral scramble NELL-1 group had marked decreases in the G0/G1 and S phase cell populations compared to the NELL-1 treatment group. This may have occurred due to some commonly observed off-target effects of lentiviral infection[63], even though we used a similar M2 cell lines with 90% knockdown efficiency generated from our previous work[10]. RT-PCR analysis

of Ki67, a cell proliferation marker, showed similar trends. After 3 days of osteogenic induction, cell proliferation increased in the NELL-1 and PPARγ knockdown groups. The addition of NELL-1 in the PPARγ knockdown cell culture significantly elevated Ki67 mRNA expression levels compared to the single agent NELL-1 or PPARγ knockdown treatment groups (Figure S4C). Annexin V-PI staining demonstrated that the NELL-1 and srPPARγ treatments attenuated the percentage of early apoptotic cells (Figure S5A). Comprehensively, adding NELL-1 to the srPPARγ-treated cells did not appear to impact the early apoptotic cell population significantly compared to the srPPARγ or NELL-1 treatments alone (Figure S5B). However, the addition of NELL-1 to the srPPARγ-treated cells significantly attenuated late apoptotic cells compared to the srPPARγ or NELL-1 treatments alone (Figure S5C).

DISCUSSION

Emerging evidence suggests that PPARγ, a nuclear receptor and transcription factor, plays essential roles in regulating bone marrow adipogenesis and osteoblastogenesis[1, 4, 7, 8, 64, 65]. In many studies, PPARγ has been shown to operate as a positive regulator for bone marrow adipogenesis and negative modulator of Wnt/β-catenin target genes, which has previously been found to result in increased bone marrow adipocyte accumulation at the expense of osteoblastogenesis[1, 4, 7, 8, 64, 65]. Akune *et al* demonstrated that embryonic stem cells derived from *PPARγ−/−* mice had significantly enhanced osteogenesis with suppressed adipogenesis[66]. This phenomenon was reversed by adding a PPARγ retroviral vector into the cell culture[66]. However, in some studies[67], such as our previous work that combined BMP2 with a srPPARγ lentiviral vector[10], adipogenic and osteoblastic differentiation can occur independently and suppressing adipogenesis may not necessarily enhance bone regeneration. These findings suggest that there may be separate regulatory mechanisms or different pools of progenitor cells that can contribute to osteoblastic and adipocytic lineage differentiation[68]. To further understand the mechanisms behind PPARγ's contributions to bone metabolism regulation, we used a lentiviral PPARγ shRNA vector delivered via femoral intramedullary injection in young adult SCID mice[59]. For clinical feasibility, we utilized immunocompetent senile osteopenic mice with intramedullary injections of BADGE, a synthetic antagonist of PPARγ, to suppress PPARγ from stimulating adipocyte differentiation[69]. With these two distinct approaches, we aimed to explore the effects of PPARγ suppression treatment and further examine the bone formation effects of combining PPARγ suppression treatment with NELL-1 protein, a Wnt modulator.

Unlike its well-established osteogenic effects, NELL-1's function in regulating lipid metabolism requires further investigation. Several genome-wide association and gene expression analyses have implicated NELL-1 in the context of lipogenesis and lipid metabolism[70–72]. In accordance with our preliminary studies, our current results revealed that using either srPPARγ or NELL-1 treatments alone could suppress adipogenesis[27, 59]. Additionally, we found that NELL-1's anti-adipogenic effect worked in a dose-dependent manner. In contrast to the findings from our previous study that utilized co-treatment with srPPARy and BMP2 in bone defects[10], we discovered that srPPARγ enhances NELL-1 or NELL-PEG's bone formation capacities, expression of the osteogenic markers OCN

and RUNX2, and β-catenin staining. More importantly, the addition of BADGE to the NELL-PEG treatment showed similar results to the combined NELL-PEG + srPPARγ treatment in enhancing osteogenesis and mineralization. Still, the combination treatments did not further decrease bone resorption and adipogenesis compared to the single agent NELL-1 treatment. Our findings pertaining to PPARγ suppression on normal osteoclastic activity is in agreement with findings from heterozygous PPARγ-deficient mice exhibiting increased BMD and osteoblast differentiation with normal osteoclast function that have been previously described[66]. We also found that single agent BADGE or NELL-PEG injections were able to suppress adipogenesis in osteopenic mice and enhance osteogenesis 8 weeks post-injection, which is supported by a previous study that showed treatment with BADGE improved BMD and decreased marrow adiposity in adult mice[73]. Despite these promising findings, another group reported that BADGE treatment did not promote osteogenesis in human MSCs[67], though the bone marrow fat formation was significantly suppressed[67]. Several reports have suggested that the administration of selective PPARγ-ligand inhibitors may contribute to the variation in the reported results, which may depend on several factors such as cell-type specificity, dosage, administration regimen, and ligand binding properties[68, 74, 75]. The literature has yet to reach a consensus on PPARγ activity on osteogenesis, adipogenesis, and osteoclastogenesis[68, 74, 75]. This may explain why one study reported that PPARγ activation inhibits osteoclast precursor cell differentiation[68], while another research reported that PPARγ activation indirectly induces expression of PGC1β, a PPARγ coactivator, that in turn stimulates osteoclastogenesis[76]. Duque *et* al[73] suggested that PPARγ inhibitors may act through a PPARγ-dependent mechanism; therefore, BADGE treatment could increase osteoblastic activities and decrease PPARγ protein expression without any alteration in osteoclastic activities[73]. Interestingly, their experiments also revealed that the combination of BADGE + vitamin D a did not show significant differences in PPARγ protein level when compared with treatment using BADGE alone[73]. These findings are similar to ours, in that both PPARγ suppression and NELL-1 may work through a similar axis of mechanism within the PPARγ/CEBPα pathway. Thus, the co-treatment of PPARγ suppression and NELL-1 stimulation enhanced the *in vitro* mineralization of primary BMSCs, M2 cells, and new bone formation in both animal models, though the inhibitory effects on bone resorption and adipogenic differentiation were not reduced more than using either of the single agent treatments alone.

In addition to acting as an adipogenic regulator, PPARγ has been widely implicated in cancer cell activity due to its effects mediating cell proliferation, differentiation, apoptosis, and metabolic homeostasis. Many PPARγ ligands, particularly thiazolidinedione agents, have been explored as anti-cancer therapies due to their pro-apoptotic and anti-proliferation properties. Depending on cell type, these ligands have been found to induce apoptosis or cell proliferation in a PPARγ-dependent or independent manner[77–80]. In this study, we explored the effect of PPARγ combination treatment on apoptosis and cell proliferation in BMSCs. The annexin V and PI analyses showed significantly decreased cell populations due to early apoptosis in all of the NELL-1-treated groups compared to the PBS-treated groups. Co-treatment with srPPARγ + NELL-1 significantly reduced the late apoptotic cell population by approximately 52% compared to the PBS or srSC + PBS groups, and an approximate 35% decrease compared to the other treatment groups. Similarly, using

BMSCs isolated from osteopenic mice had no significant difference in early apoptosis among the BADGE, NELL-PEG, and NELL-PEG + BADGE treatment groups. Only late apoptosis decreased significantly with NELL-PEG + BADGE co-treatment. These findings may indicate that knocking down or inhibiting PPARγ exerts an anti-apoptotic effect on BMSCs, while the combination of PPARγ suppression + NELL-1 further enhances NELL-1's protective effects against BMSC apoptosis. To elucidate factors that are affected by this co-treatment, several assays, including cyclin-dependent kinase (CDK) activity assays[81], time-course analyses[82], and caspase assays[82], warrant consideration for future investigation. Using primary BMSCs and the M2 murine bone marrow cell line, our cell proliferation analysis demonstrated that PPARγ suppression + NELL-1 co-treatment significantly increased the cell population in S phase compared to the other treatment groups, while the cell population in the G0/G1 group was significantly decreased. Additionally, the mRNA expression level of a nuclear protein associated with cell proliferation and ribosomal RNA transcription, Ki67, was also increased. The cell cycle and RT-PCR analysis results suggest that co-treatment with PPARγ suppression + NELL-1 may be an effective approach to stimulate cell proliferation. Furthermore, this co-treatment strategy also significantly improved mineralization without altering the single agent effects on adipogenesis suppression and bone resorption. Based on our findings, the co-treatment with PPARγ suppression + NELL-1 showed therapeutic potential for mitigating BMSC apoptosis and growth.

CONCLUSIONS

In summation, the current study demonstrates that the addition of PPARγ suppression to NELL-1 therapy can be an effective approach to enhance NELL-1's effects on bone formation by upregulating anabolic processes without significantly altering NELL-1's inhibitory effects on osteoclastic and adipogenic activities. Both methods of PPARγ suppression increased osteogenic marker levels and decreased adipogenic marker expression levels. The combination therapy additively increased osteogenic marker expression levels compared to the single treatment groups, whereas the adipogenic marker expression levels were maintained at similar quantities to those in the single treatment groups. Ultimately, the goal of combining an osteogenic molecule with a small molecule inhibitor or pharmaceutical compound is to create a viable therapeutic that enhances bone regeneration with respect to production cost of currently available medication, as creating native protein molecules requires laborious biological synthesis processes[83]. Future directions will focus on characterizing NELL-1's effect on the PPARγ and Wnt/β-catenin pathways within an extremely challenging setting, such as the microgravity-induced rapid bone loss, to elucidate new mechanisms that are involved in regulating the balance between bone regeneration and bone marrow adipogenesis.

Supplementary Material

Refer to Web version on PubMed Central for supplementary material.

ACKNOWLEDGEMENTS

This work is supported by the California Institute for Regenerative Medicine Early Translational II Research award TR2-01821 (C.S.), NIH/National Institute of Dental and Craniofacial Research grant R21 DE0177711 (C.S.), NIH/NIAMS grants R01 AR061399-02 (C.S.), R01 AR066782-01 (K.T.), R01 AR068835-01A1 (C.S.), RO1 DE029353 (C.S. and X.Z.), University of California Discovery grant 07-10677 (B.W., C.S., and X.Z.), and the Eli and Edythe Broad Center of Regenerative Medicine and Stem Cell Research at the University of California, Los Angeles Innovation award (C.S.) CTSI UL1TR000124 (sub-award to X.Z.). The authors would like to thank N.G., S.L., and Y.M. for their general assistance.

List of abbreviation

PPARy	Peroxisome proliferator-activated receptor gamma
PPARy-shRNA	Peroxisome proliferator-activated receptor gamma small hairpin RNA
BMP2	Bone morphogenetic protein-2
Wnt	Wingless and Int-1
NELL-1	Neural Epidermal Growth Factor Like 1
NELL-PEG	PEGylated NELL-1
OVX	Ovariectomized
Cntnap4	Contactin-associated protein-like 4
MAPK/JNK	Mitogen activated protein kinase / Jun N-terminal kinase
HH	Hedgehog
FDA	Food and Drug Administration
ARC	Animal Research Committee
SCID	Severe combined immunodeficiency
MOI	Multiplicity of Infection
BADGE	Bisphenol A diglycidyl ether
TCID	Tissue culture infective dosage
BMD	Bone mineral density
ROI	Region of interest
EDTA	Ethylenediaminetetraacetic acid
ABC	Avidin-biotin complex
IHC	Immunohistochemistry
AEC	Amino ethyl carbazole

OCN	Osteocalcin
TRAP	Tartrate-resistant acid phosphatase
BMSC	Bone marrow-derived stem cell
M2	M2–10B4 cell line
RPMI	Roswell Park Memorial Institute
M2-PP	Selected M2–10B4 clonal cells treated with lentiviral PPARγ knockdown
M2-SC	Selected M2–10B4 clonal cells treated with lentiviral scramble
DMEM	Dulbecco's Modified Eagle Medium
FBS	Fetal bovine serum
PBS	Phosphate-buffered saline
FITC	Fluorescein isothiocyanate
BrdU	Bromodeoxyuridine
7-AAD	7-Aminoactinomycin D
IP	Intraperitoneal
FACS	Fluorescence-activated cell sorting
RT-PCR	Real-time polymerase chain reaction
PPARγ2	Peroxisome proliferator-activated receptor γ2
RUNX2	Runt-related transcription factor 2
CEBPa	CCAAT/enhancer-binding protein alpha
Ki67	Nuclear protein Ki67
GADPH	Glyceraldehyde 3-phosphate dehydrogenase
CI	Confidence intervals
SD	Standard deviation
SEM	Standard error of the mean
microCT	Micro Computed Tomography
DXA	Dual-energy x-ray absorptiometry
TMD	Tissue Mineral Density
BV	Bone Volume

TV	Tissue Volume
MS	Midshaft
DS	Distal Shaft
AD	Adipogenic differentiation
OD	Osteogenic differentiation

REFERENCES

[1]. Siersbaek R, Nielsen R, Mandrup S, PPARgamma in adipocyte differentiation and metabolism--novel insights from genome-wide studies, FEBS Lett 584(15) (2010) 3242–9. [PubMed: 20542036]

[2]. Farmer SR, Regulation of PPARgamma activity during adipogenesis, Int J Obes (Lond) 29 Suppl 1 (2005) S13–6. [PubMed: 15711576]

[3]. Patel JJ, Butters OR, Arnett TR, PPAR agonists stimulate adipogenesis at the expense of osteoblast differentiation while inhibiting osteoclast formation and activity, Cell Biochem Funct 32(4) (2014) 368–77. [PubMed: 24615887]

[4]. Wan Y, Chong LW, Evans RM, PPAR-gamma regulates osteoclastogenesis in mice, Nat Med 13(12) (2007) 1496–503. [PubMed: 18059282]

[5]. Stechschulte LA, Czernik PJ, Rotter ZC, Tausif FN, Corzo CA, Marciano DP, Asteian A, Zheng J, Bruning JB, Kamenecka TM, Rosen CJ, Griffin PR, Lecka-Czernik B, PPARG Post-translational Modifications Regulate Bone Formation and Bone Resorption, EBioMedicine 10 (2016) 174–84. [PubMed: 27422345]

[6]. Pei L, Tontonoz P, Fat's loss is bone's gain, J Clin Invest 113(6) (2004) 805–6. [PubMed: 15067310]

[7]. Takada I, Kouzmenko AP, Kato S, Wnt and PPARgamma signaling in osteoblastogenesis and adipogenesis, Nat Rev Rheumatol 5(8) (2009) 442–7. [PubMed: 19581903]

[8]. Takada I, Suzawa M, Matsumoto K, Kato S, Suppression of PPAR transactivation switches cell fate of bone marrow stem cells from adipocytes into osteoblasts, Ann N Y Acad Sci 1116 (2007) 182–95. [PubMed: 17656564]

[9]. James AW, Pan A, Chiang M, Zara JN, Zhang X, Ting K, Soo C, A new function of Nell-1 protein in repressing adipogenic differentiation, Biochem Biophys Res Commun 411(1) (2011) 126–31. [PubMed: 21723263]

[10]. Wang C, Tanjaya J, Shen J, Lee S, Bisht B, Pan HC, Pang S, Zhang Y, Berthiaume EA, Chen E, Da Lio AL, Zhang X, Ting K, Guo S, Soo C, Peroxisome Proliferator-Activated Receptor-gamma Knockdown Impairs Bone Morphogenetic Protein-2-Induced Critical-Size Bone Defect Repair, Am J Pathol 189(3) (2019) 648–664. [PubMed: 30593824]

[11]. Kobayashi M, Funayama R, Ohnuma S, Unno M, Nakayama K, Wnt-beta-catenin signaling regulates ABCC3 (MRP3) transporter expression in colorectal cancer, Cancer Sci 107(12) (2016) 1776–1784. [PubMed: 27709738]

[12]. Kramer I, Halleux C, Keller H, Pegurri M, Gooi JH, Weber PB, Feng JQ, Bonewald LF, Kneissel M, Osteocyte Wnt/beta-catenin signaling is required for normal bone homeostasis, Mol Cell Biol 30(12) (2010) 3071–85. [PubMed: 20404086]

[13]. Gao C, Xiao G, Hu J, Regulation of Wnt/beta-catenin signaling by posttranslational modifications, Cell Biosci 4(1) (2014) 13. [PubMed: 24594309]

[14]. Kobayashi Y, Uehara S, Udagawa N, Takahashi N, Regulation of bone metabolism by Wnt signals, J Biochem 159(4) (2016) 387–92. [PubMed: 26711238]

[15]. van Noort M, Meeldijk J, van der Zee R, Destree O, Clevers H, Wnt signaling controls the phosphorylation status of beta-catenin, J Biol Chem 277(20) (2002) 17901–5. [PubMed: 11834740]

[16]. Aghaloo T, Cowan CM, Chou YF, Zhang X, Lee H, Miao S, Hong N, Kuroda S, Wu B, Ting K, Soo C, Nell-1-induced bone regeneration in calvarial defects, Am J Pathol 169(3) (2006) 903–15. [PubMed: 16936265]

[17]. Aghaloo T, Jiang X, Soo C, Zhang Z, Zhang X, Hu J, Pan H, Hsu T, Wu B, Ting K, Zhang X, A study of the role of nell-1 gene modified goat bone marrow stromal cells in promoting new bone formation, Mol Ther 15(10) (2007) 1872–80. [PubMed: 17653100]

[18]. Chen F, Walder B, James AW, Soofer DE, Soo C, Ting K, Zhang X, NELL-1-dependent mineralisation of Saos-2 human osteosarcoma cells is mediated via c-Jun N-terminal kinase pathway activation, Int Orthop 36(10) (2012) 2181–7. [PubMed: 22797704]

[19]. Chen W, Zhang X, Siu RK, Chen F, Shen J, Zara JN, Culiat CT, Tetradis S, Ting K, Soo C, Nfatc2 is a primary response gene of Nell-1 regulating chondrogenesis in ATDC5 cells, J Bone Miner Res 26(6) (2011) 1230–41. [PubMed: 21611965]

[20]. Cowan CM, Jiang X, Hsu T, Soo C, Zhang B, Wang JZ, Kuroda S, Wu B, Zhang Z, Zhang X, Ting K, Synergistic effects of Nell-1 and BMP-2 on the osteogenic differentiation of myoblasts, J Bone Miner Res 22(6) (2007) 918–30. [PubMed: 17352654]

[21]. Cowan CM, Zhang X, James AW, Kim TM, Sun N, Wu B, Ting K, Soo C, NELL-1 increases pre-osteoblast mineralization using both phosphate transporter Pit1 and Pit2, Biochem Biophys Res Commun 422(3) (2012) 351–7. [PubMed: 22580275]

[22]. James AW, Chiang M, Asatrian G, Shen J, Goyal R, Chung CG, Chang L, Shrestha S, Turner AS, Seim HB 3rd, Zhang X, Wu BM, Ting K, Soo C, Vertebral Implantation of NELL-1 Enhances Bone Formation in an Osteoporotic Sheep Model, Tissue Eng Part A 22(11–12) (2016) 840–9. [PubMed: 27113550]

[23]. James AW, Pang S, Askarinam A, Corselli M, Zara JN, Goyal R, Chang L, Pan A, Shen J, Yuan W, Stoker D, Zhang X, Adams JS, Ting K, Soo C, Additive effects of sonic hedgehog and Nell-1 signaling in osteogenic versus adipogenic differentiation of human adipose-derived stromal cells, Stem Cells Dev 21(12) (2012) 2170–8. [PubMed: 22264144]

[24]. James AW, Shen J, Tsuei R, Nguyen A, Khadarian K, Meyers CA, Pan HC, Li W, Kwak JH, Asatrian G, Culiat CT, Lee M, Ting K, Zhang X, Soo C, NELL-1 induces Sca-1+ mesenchymal progenitor cell expansion in models of bone maintenance and repair, JCI Insight 2(12) (2017).

[25]. James AW, Shen J, Zhang X, Asatrian G, Goyal R, Kwak JH, Jiang L, Bengs B, Culiat CT, Turner AS, Seim Iii HB, Wu BM, Lyons K, Adams JS, Ting K, Soo C, NELL-1 in the treatment of osteoporotic bone loss, Nat Commun 6 (2015) 7362. [PubMed: 26082355]

[26]. Kwak J, Zara JN, Chiang M, Ngo R, Shen J, James AW, Le KM, Moon C, Zhang X, Gou Z, Ting K, Soo C, NELL-1 injection maintains long-bone quantity and quality in an ovariectomy-induced osteoporotic senile rat model, Tissue Eng Part A 19(3–4) (2013) 426–36. [PubMed: 23083222]

[27]. Kwak JH, Zhang Y, Park J, Chen E, Shen J, Chawan C, Tanjaya J, Lee S, Zhang X, Wu BM, Ting K, Soo C, Pharmacokinetics and osteogenic potential of PEGylated NELL-1 in vivo after systemic administration, Biomaterials 57 (2015) 73–83. [PubMed: 25913252]

[28]. Lee M, Siu RK, Ting K, Wu BM, Effect of Nell-1 delivery on chondrocyte proliferation and cartilaginous extracellular matrix deposition, Tissue Eng Part A 16(5) (2010) 1791–800. [PubMed: 20028218]

[29]. Li C, Zhang X, Zheng Z, Nguyen A, Ting K, Soo C, Nell-1 Is a Key Functional Modulator in Osteochondrogenesis and Beyond, J Dent Res 98(13) (2019) 1458–1468. [PubMed: 31610747]

[30]. Li CS, Zhang X, Peault B, Jiang J, Ting K, Soo C, Zhou YH, Accelerated Chondrogenic Differentiation of Human Perivascular Stem Cells with NELL-1, Tissue Eng Part A 22(3–4) (2016) 272–85. [PubMed: 26700847]

[31]. Li W, Lee M, Whang J, Siu RK, Zhang X, Liu C, Wu BM, Wang JC, Ting K, Soo C, Delivery of lyophilized Nell-1 in a rat spinal fusion model, Tissue Eng Part A 16(9) (2010) 2861–70. [PubMed: 20528102]

[32]. Li W, Zara JN, Siu RK, Lee M, Aghaloo T, Zhang X, Wu BM, Gertzman AA, Ting K, Soo C, Nell-1 enhances bone regeneration in a rat critical-sized femoral segmental defect model, Plast Reconstr Surg 127(2) (2011) 580–7. [PubMed: 21285762]

[33]. Lu SS, Zhang X, Soo C, Hsu T, Napoli A, Aghaloo T, Wu BM, Tsou P, Ting K, Wang JC, The osteoinductive properties of Nell-1 in a rat spinal fusion model, Spine J 7(1) (2007) 50–60. [PubMed: 17197333]

[34]. Pang S, Shen J, Liu Y, Chen F, Zheng Z, James AW, Hsu CY, Zhang H, Lee KS, Wang C, Li C, Chen X, Jia H, Zhang X, Soo C, Ting K, Proliferation and osteogenic differentiation of mesenchymal stem cells induced by a short isoform of NELL-1, Stem Cells 33(3) (2015) 904–15. [PubMed: 25376942]

[35]. Qin XY, Zhao HX, Zhang Q, Chen F, Lin JX, [NELL-1: a novel highly efficient and specific growth factor], Beijing Da Xue Xue Bao Yi Xue Ban 48(2) (2016) 380–3. [PubMed: 27080300]

[36]. Shen J, James AW, Chung J, Lee K, Zhang JB, Ho S, Lee KS, Kim TM, Niimi T, Kuroda S, Ting K, Soo C, NELL-1 promotes cell adhesion and differentiation via Integrinbeta1, J Cell Biochem 113(12) (2012) 3620–8. [PubMed: 22807400]

[37]. Shen J, LaChaud G, Khadarian K, Shrestha S, Zhang X, Soo C, Ting K, Dry SM, James AW, NELL-1 expression in benign and malignant bone tumors, Biochem Biophys Res Commun 460(2) (2015) 368–74. [PubMed: 25791475]

[38]. Shen J, LaChaud G, Shrestha S, Asatrian G, Zhang X, Dry SM, Soo C, Ting K, James AW, NELL-1 expression in tumors of cartilage, J Orthop 12(Suppl 2) (2015) S223–9. [PubMed: 27047227]

[39]. Siu RK, Lu SS, Li W, Whang J, McNeill G, Zhang X, Wu BM, Turner AS, Seim HB 3rd, Hoang P, Wang JC, Gertzman AA, Ting K, Soo C, Nell-1 protein promotes bone formation in a sheep spinal fusion model, Tissue Eng Part A 17(7–8) (2011) 1123–35. [PubMed: 21128865]

[40]. Siu RK, Zara JN, Hou Y, James AW, Kwak J, Zhang X, Ting K, Wu BM, Soo C, Lee M, NELL-1 promotes cartilage regeneration in an in vivo rabbit model, Tissue Eng Part A 18(3–4) (2012) 252–61. [PubMed: 21902605]

[41]. Tanjaya J, Lord EL, Wang C, Zhang Y, Kim JK, Nguyen A, Baik L, Pan HC, Chen E, Kwak JH, Zhang X, Wu B, Soo C, Ting K, The Effects of Systemic Therapy of PEGylated NEL-Like Protein 1 (NELL-1) on Fracture Healing in Mice, Am J Pathol 188(3) (2018) 715–727. [PubMed: 29294300]

[42]. Tanjaya J, Zhang Y, Lee S, Shi J, Chen E, Ang P, Zhang X, Tetradis S, Ting K, Wu B, Soo C, Kwak JH, Efficacy of Intraperitoneal Administration of PEGylated NELL-1 for Bone Formation, Biores Open Access 5(1) (2016) 159–70. [PubMed: 27354930]

[43]. Ting K, Vastardis H, Mulliken JB, Soo C, Tieu A, Do H, Kwong E, Bertolami CN, Kawamoto H, Kuroda S, Longaker MT, Human NELL-1 expressed in unilateral coronal synostosis, J Bone Miner Res 14(1) (1999) 80–9. [PubMed: 9893069]

[44]. Yuan W, James AW, Asatrian G, Shen J, Zara JN, Tian HJ, Siu RK, Zhang X, Wang JC, Dong J, NELL-1 based demineralized bone graft promotes rat spine fusion as compared to commercially available BMP-2 product, J Orthop Sci 18(4) (2013) 646–57. [PubMed: 23686083]

[45]. Zhang X, Peault B, Chen W, Li W, Corselli M, James AW, Lee M, Siu RK, Shen P, Zheng Z, Shen J, Kwak J, Zara JN, Chen F, Zhang H, Yin Z, Wu B, Ting K, Soo C, The Nell-1 growth factor stimulates bone formation by purified human perivascular cells, Tissue Eng Part A 17(19–20) (2011) 2497–509. [PubMed: 21615216]

[46]. Zhang X, Ting K, Pathmanathan D, Ko T, Chen W, Chen F, Lee H, James AW, Siu RK, Shen J, Culiat CT, Soo C, Calvarial cleidocraniodysplasia-like defects with ENU-induced Nell-1 deficiency, J Craniofac Surg 23(1) (2012) 61–6. [PubMed: 22337375]

[47]. Zhang X, Zara J, Siu RK, Ting K, Soo C, The role of NELL-1, a growth factor associated with craniosynostosis, in promoting bone regeneration, J Dent Res 89(9) (2010) 865–78. [PubMed: 20647499]

[48]. Zhang Y, Dong R, Park Y, Bohner M, Zhang X, Ting K, Soo C, Wu BM, Controlled release of NELL-1 protein from chitosan/hydroxyapatite-modified TCP particles, Int J Pharm 511(1) (2016) 79–89. [PubMed: 27349789]

[49]. Zhang Y, Velasco O, Zhang X, Ting K, Soo C, Wu BM, Bioactivity and circulation time of PEGylated NELL-1 in mice and the potential for osteoporosis therapy, Biomaterials 35(24) (2014) 6614–21. [PubMed: 24818884]

[50]. Xia L, Xu Y, Chang Q, Sun X, Zeng D, Zhang W, Zhang X, Zhang Z, Jiang X, Maxillary sinus floor elevation using BMP-2 and Nell-1 gene-modified bone marrow stromal cells and TCP in rabbits, Calcif Tissue Int 89(1) (2011) 53–64. [PubMed: 21584647]

[51]. Zhang J, Chen Y, Xu J, Wang J, Li C, Wang L, Tissue engineering using 3D printed nano-bioactive glass loaded with NELL1 gene for repairing alveolar bone defects, Regen Biomater 5(4) (2018) 213–220. [PubMed: 30094060]

[52]. Xue J, Peng J, Yuan M, Wang A, Zhang L, Liu S, Fan M, Wang Y, Xu W, Ting K, Zhang X, Lu S, NELL1 promotes high-quality bone regeneration in rat femoral distraction osteogenesis model, Bone 48(3) (2011) 485–95. [PubMed: 20959151]

[53]. Zhu S, Song D, Jiang X, Zhou H, Hu J, Combined effects of recombinant human BMP-2 and Nell-1 on bone regeneration in rapid distraction osteogenesis of rabbit tibia, Injury 42(12) (2011) 1467–73. [PubMed: 21703614]

[54]. Lee S, Zhang X, Shen J, James AW, Chung CG, Hardy R, Li C, Girgius C, Zhang Y, Stoker D, Wang H, Wu BM, Peault B, Ting K, Soo C, Brief Report: Human Perivascular Stem Cells and Nel-Like Protein-1 Synergistically Enhance Spinal Fusion in Osteoporotic Rats, Stem Cells 33(10) (2015) 3158–63. [PubMed: 26173400]

[55]. Shen J, James AW, Zara JN, Asatrian G, Khadarian K, Zhang JB, Ho S, Kim HJ, Ting K, Soo C, BMP2-induced inflammation can be suppressed by the osteoinductive growth factor NELL-1, Tissue Eng Part A 19(21–22) (2013) 2390–401. [PubMed: 23758588]

[56]. James AW, LaChaud G, Shen J, Asatrian G, Nguyen V, Zhang X, Ting K, Soo C, A Review of the Clinical Side Effects of Bone Morphogenetic Protein-2, Tissue Eng Part B Rev 22(4) (2016) 284–97. [PubMed: 26857241]

[57]. Shen J, James AW, Zhang X, Pang S, Zara JN, Asatrian G, Chiang M, Lee M, Khadarian K, Nguyen A, Lee KS, Siu RK, Tetradis S, Ting K, Soo C, Novel Wnt Regulator NEL-Like Molecule-1 Antagonizes Adipogenesis and Augments Osteogenesis Induced by Bone Morphogenetic Protein 2, Am J Pathol 186(2) (2016) 419–34. [PubMed: 26772960]

[58]. Chamorro-Garcia R, Kirchner S, Li X, Janesick A, Casey SC, Chow C, Blumberg B, Bisphenol A diglycidyl ether induces adipogenic differentiation of multipotent stromal stem cells through a peroxisome proliferator-activated receptor gamma-independent mechanism, Environ Health Perspect 120(7) (2012) 984–9. [PubMed: 22763116]

[59]. James AW, Shen J, Khadarian K, Pang S, Chung G, Goyal R, Asatrian G, Velasco O, Kim J, Zhang X, Ting K, Soo C, Lentiviral delivery of PPARgamma shRNA alters the balance of osteogenesis and adipogenesis, improving bone microarchitecture, Tissue Eng Part A 20(19–20) (2014) 2699–710. [PubMed: 24785569]

[60]. Shi J, Lee S, Uyeda M, Tanjaya J, Kim JK, Pan HC, Reese P, Stodieck L, Lin A, Ting K, Kwak JH, Soo C, Guidelines for Dual Energy X-Ray Absorptiometry Analysis of Trabecular Bone-Rich Regions in Mice: Improved Precision, Accuracy, and Sensitivity for Assessing Longitudinal Bone Changes, Tissue Eng Part C Methods 22(5) (2016) 451–63. [PubMed: 26956416]

[61]. Iezzi I, Cerqueni G, Licini C, Lucarini G, Mattioli Belmonte M, Dental pulp stem cells senescence and regenerative potential relationship, J Cell Physiol 234(5) (2019) 7186–7197. [PubMed: 30362542]

[62]. Jilka RL, The relevance of mouse models for investigating age-related bone loss in humans, J Gerontol A Biol Sci Med Sci 68(10) (2013) 1209–17. [PubMed: 23689830]

[63]. Milone MC, O'Doherty U, Clinical use of lentiviral vectors, Leukemia 32(7) (2018) 1529–1541. [PubMed: 29654266]

[64]. Demontiero O, Vidal C, Duque G, Aging and bone loss: new insights for the clinician, Ther Adv Musculoskelet Dis 4(2) (2012) 61–76. [PubMed: 22870496]

[65]. Lehrke M, Lazar MA, The many faces of PPARgamma, Cell 123(6) (2005) 993–9. [PubMed: 16360030]

[66]. Akune T, Ohba S, Kamekura S, Yamaguchi M, Chung UI, Kubota N, Terauchi Y, Harada Y, Azuma Y, Nakamura K, Kadowaki T, Kawaguchi H, PPARgamma insufficiency enhances osteogenesis through osteoblast formation from bone marrow progenitors, J Clin Invest 113(6) (2004) 846–55. [PubMed: 15067317]

[67]. Yu WH LF, Chen XY, Li JT, Wu YH, Huang LH, Wang Z, Li P, Wang T, Lahn BT, Xiang AP, PPARgamma suppression inhibits adipogenesis but does not promote osteogenesis of human mesenchymal stem cells, 44(2) (2012) 377–84. [PubMed: 22120652]

[68]. Lecka-Czernik B, Suva LJ, Resolving the Two "Bony" Faces of PPAR-gamma, PPAR Res 2006 (2006) 27489. [PubMed: 17259664]

[69]. Wright HM, Clish CB, Mikami T, Hauser S, Yanagi K, Hiramatsu R, Serhan CN, Spiegelman BM, A synthetic antagonist for the peroxisome proliferator-activated receptor gamma inhibits adipocyte differentiation, J Biol Chem 275(3) (2000) 1873–7. [PubMed: 10636887]

[70]. de Luis DA, Almansa R, Aller R, Izaola O, Romero E, Gene expression analysis identify a metabolic and cell function alterations as a hallmark of obesity without metabolic syndrome in peripheral blood, a pilot study, Clin Nutr 37(4) (2018) 1348–1353. [PubMed: 28633944]

[71]. Kraja AT, Borecki IB, Tsai MY, Ordovas JM, Hopkins PN, Lai CQ, Frazier-Wood AC, Straka RJ, Hixson JE, Province MA, Arnett DK, Genetic analysis of 16 NMR-lipoprotein fractions in humans, the GOLDN study, Lipids 48(2) (2013) 155–65. [PubMed: 23192668]

[72]. Rudkowska I, Guenard F, Julien P, Couture P, Lemieux S, Barbier O, Calder PC, Minihane AM, Vohl MC, Genome-wide association study of the plasma triglyceride response to an n-3 polyunsaturated fatty acid supplementation, J Lipid Res 55(7) (2014) 1245–53. [PubMed: 24847101]

[73]. Duque G, Li W, Vidal C, Bermeo S, Rivas D, Henderson J, Pharmacological inhibition of PPARgamma increases osteoblastogenesis and bone mass in male C57BL/6 mice, J Bone Miner Res 28(3) (2013) 639–48. [PubMed: 23044841]

[74]. Tsukahara T, The Role of PPARgamma in the Transcriptional Control by Agonists and Antagonists, PPAR Res 2012 (2012) 362361. [PubMed: 22693486]

[75]. Nakamuta M, Enjoji M, Uchimura K, Ohta S, Sugimoto R, Kotoh K, Kato M, Irie T, Muta T, Nawata H, Bisphenol a diglycidyl ether (BADGE) suppresses tumor necrosis factor-alpha production as a PPARgamma agonist in the murine macrophage-like cell line, RAW 264.7, Cell Biol Int 26(3) (2002) 235–41. [PubMed: 11991651]

[76]. Wei W, Wang X, Yang M, Smith LC, Dechow PC, Sonoda J, Evans RM, Wan Y, PGC1beta mediates PPARgamma activation of osteoclastogenesis and rosiglitazone-induced bone loss, Cell Metab 11(6) (2010) 503–16. [PubMed: 20519122]

[77]. Fehlberg S, Trautwein S, Goke A, Goke R, Bisphenol A diglycidyl ether induces apoptosis in tumour cells independently of peroxisome proliferator-activated receptor-gamma, in caspase-dependent and -independent manners, Biochem J 362(Pt 3) (2002) 573–8. [PubMed: 11879183]

[78]. Garcia-Bates TM, Bernstein SH, Phipps RP, Peroxisome proliferator-activated receptor gamma overexpression suppresses growth and induces apoptosis in human multiple myeloma cells, Clin Cancer Res 14(20) (2008) 6414–25. [PubMed: 18927280]

[79]. Lea MA, Sura M, Desbordes C, Inhibition of cell proliferation by potential peroxisome proliferator-activated receptor (PPAR) gamma agonists and antagonists, Anticancer Res 24(5A) (2004) 2765–71. [PubMed: 15517883]

[80]. Simpson-Haidaris PJ, Pollock SJ, Ramon S, Guo N, Woeller CF, Feldon SE, Phipps RP, Anticancer Role of PPARgamma Agonists in Hematological Malignancies Found in the Vasculature, Marrow, and Eyes, PPAR Res 2010 (2010) 814609. [PubMed: 20204067]

[81]. Swaffer MP, Jones AW, Flynn HR, Snijders AP, Nurse P, CDK Substrate Phosphorylation and Ordering the Cell Cycle, Cell 167(7) (2016) 1750–1761 e16. [PubMed: 27984725]

[82]. Wlodkowic D, Telford W, Skommer J, Darzynkiewicz Z, Apoptosis and beyond: cytometry in studies of programmed cell death, Methods Cell Biol 103 (2011) 55–98. [PubMed: 21722800]

[83]. Scheller EL, Krebsbach PH, The use of soluble signals to harness the power of the bone microenvironment for implant therapeutics, Int J Oral Maxillofac Implants 26 Suppl (2011) 70–9; discussion 80–4.

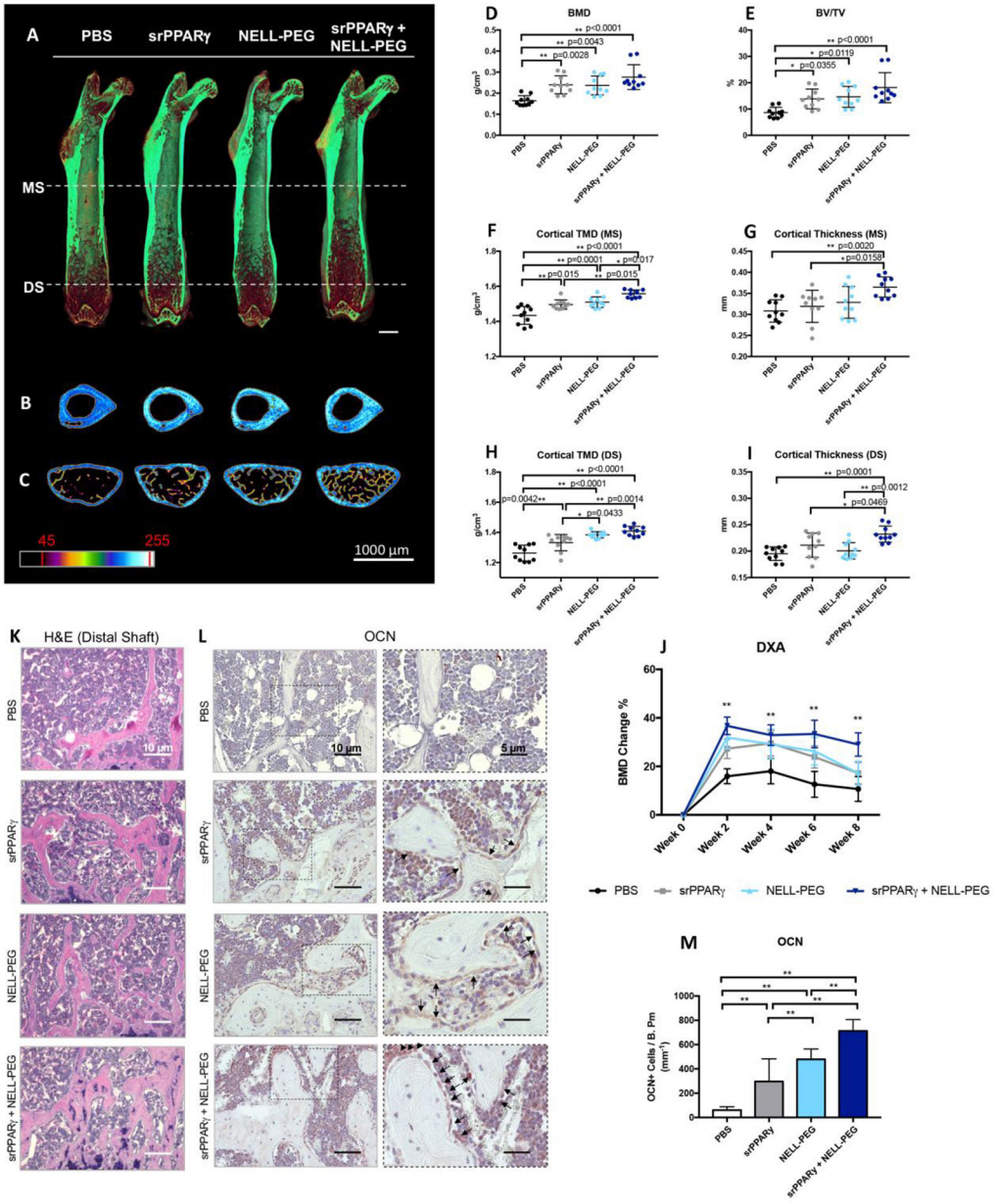

Figure 1. MicroCT and immunohistochemical analyses of trabecular bone formation in SCID mice.

(1A) Representative 3D images of treatment groups 8 weeks post-injection. (1B-C) Representative cross-sectional images of trabecular bone at the midshaft (MS) and distal shaft (DS) of the femur. (1D-E) Trabecular bone analysis revealed a significant increase in BMD and BV/TV in all treatment groups compared to the PBS group. (1F-I) Cortical bone analysis at the MS and DS showed increased TMD and cortical thickness in the co-treatment group compared to the PBS group. (1J) Longitudinal DXA analysis of %BMD change. DXA data are presented as mean ± SEM. $^{**}p<0.01$ for the srPPARγ + NELL-PEG group in comparison to the PBS group. (1K) Histological analysis of trabecular bone formation at the DS of the femur. (1L-M) Immunohistochemical staining of OCN expression and analysis. Data are presented as mean ± SD. $^{*}p<0.05$, $^{**}p<0.01$.

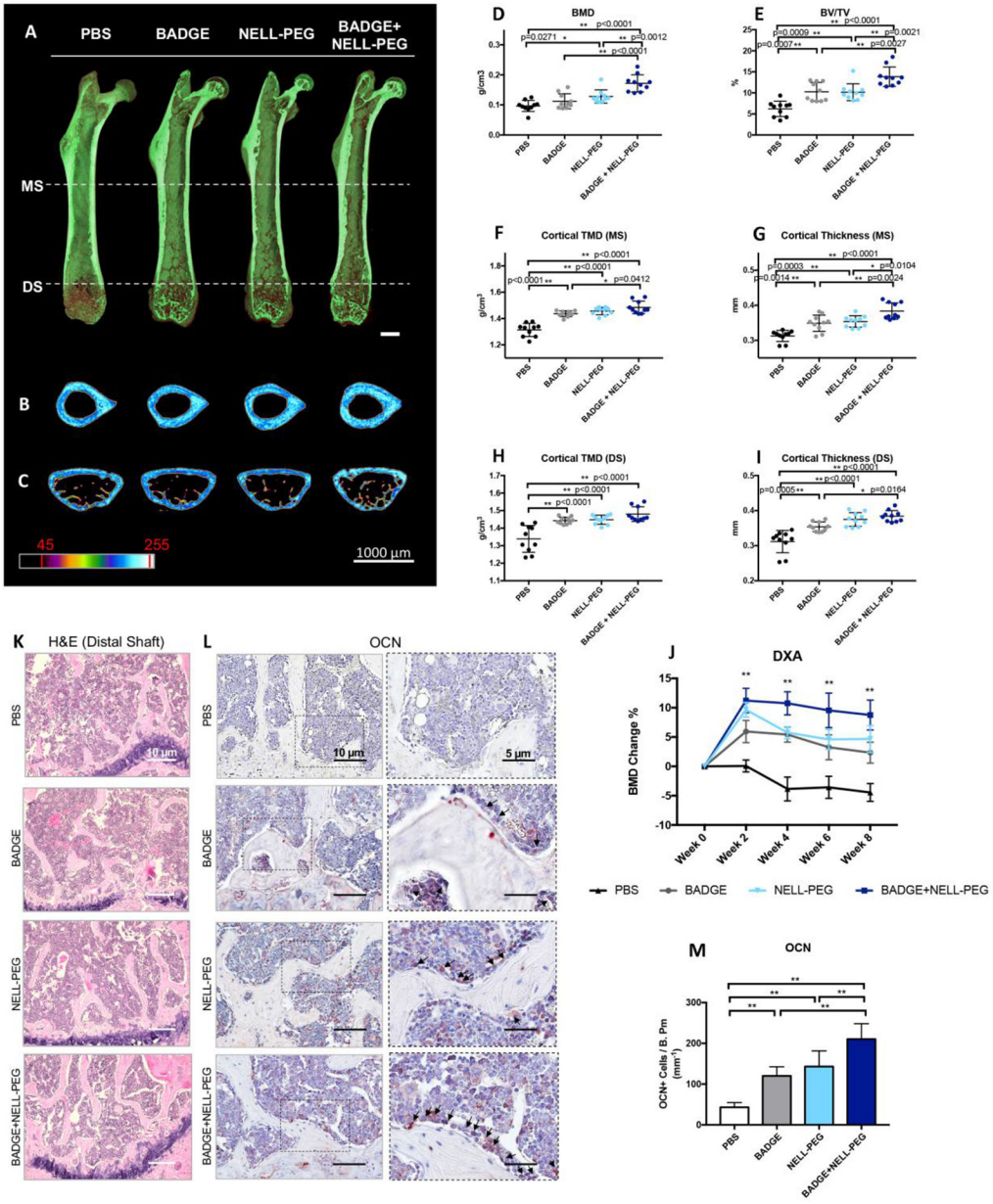

Figure 2. MicroCT and immunohistochemical analyses of trabecular bone formation in SCID and osteopenic mice.

(2A) Representative 3D images of treatment groups 8 weeks post-injection. (2B-C) Representative cross-sectional images of trabecular bone at the midshaft (MS) and distal shaft (DS) of the femur. (2D-E) Trabecular bone analysis revealed a significant increase in BMD and BV/TV in all treatment groups compared to the PBS group. (2F-I) Cortical bone analysis at the MS and DS showed increased TMD and cortical thickness in the co-treatment group compared to the PBS group. (2J) Longitudinal DXA analysis of %BMD change. DXA data are presented as mean ± SEM. $^{**}p<0.01$ for the BADGE + NELL-PEG group in comparison to the PBS group. (2K) Histological analysis of trabecular bone formation at the DS of the femur. (2L-M) Immunohistochemical staining of OCN expression and analysis. Data are presented as mean ± SD. $^{*}p<0.05$, $^{**}p<0.01$.

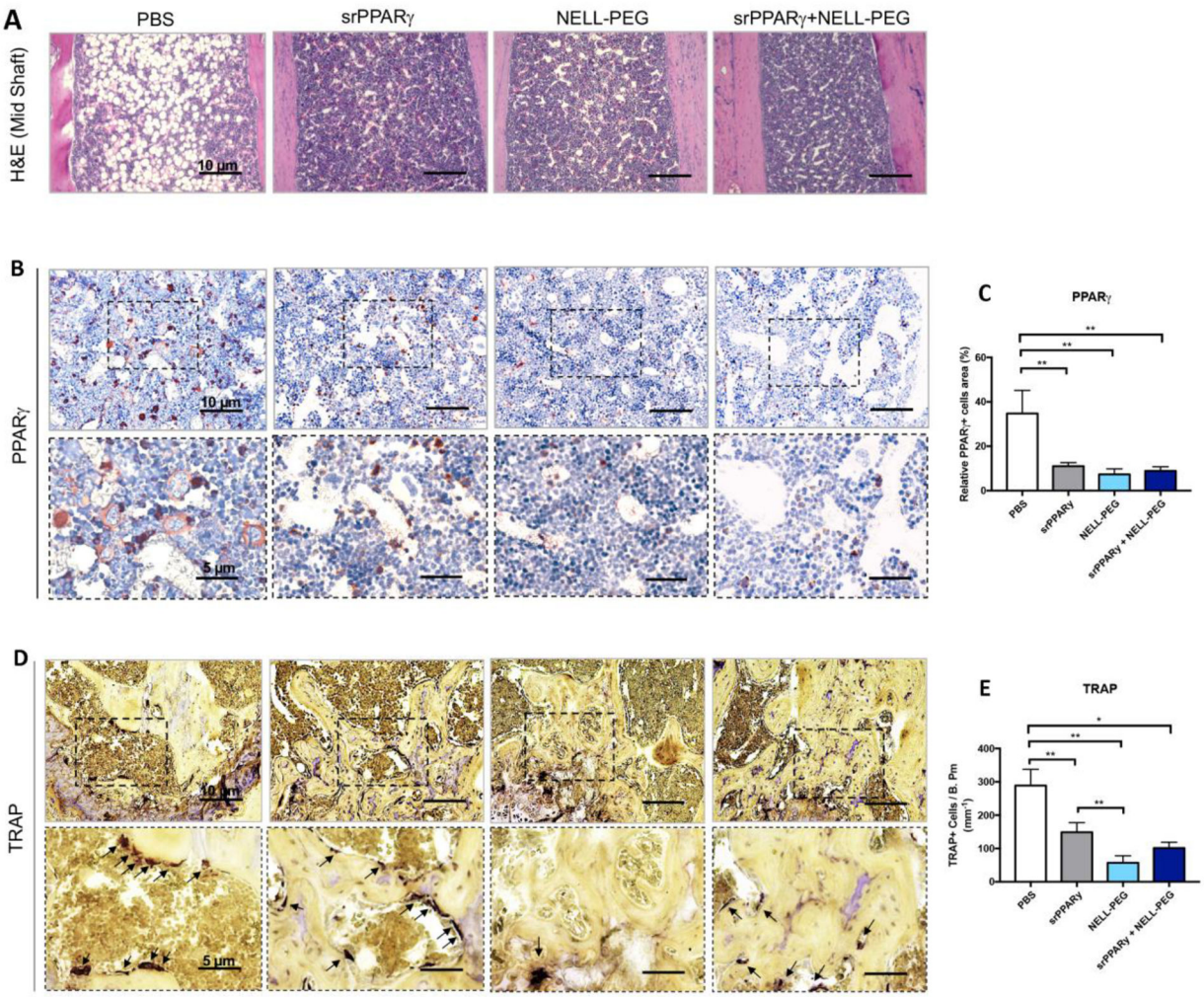

Figure 3. Histological and immunochemical analyses of bone marrow adipose formation and bone resorption in SCID mice.

(3A) H&E staining at the midshaft of the femur to examine bone marrow adipose formation. (3B-C) Immunohistochemical staining of PPARγ expression and analysis. (3D-E) TRAP immunohistochemistry and quantification of TRAP+ stained cells at the distal shaft of the femur. Data are presented as mean ± SD. *p<0.05, **p<0.01.

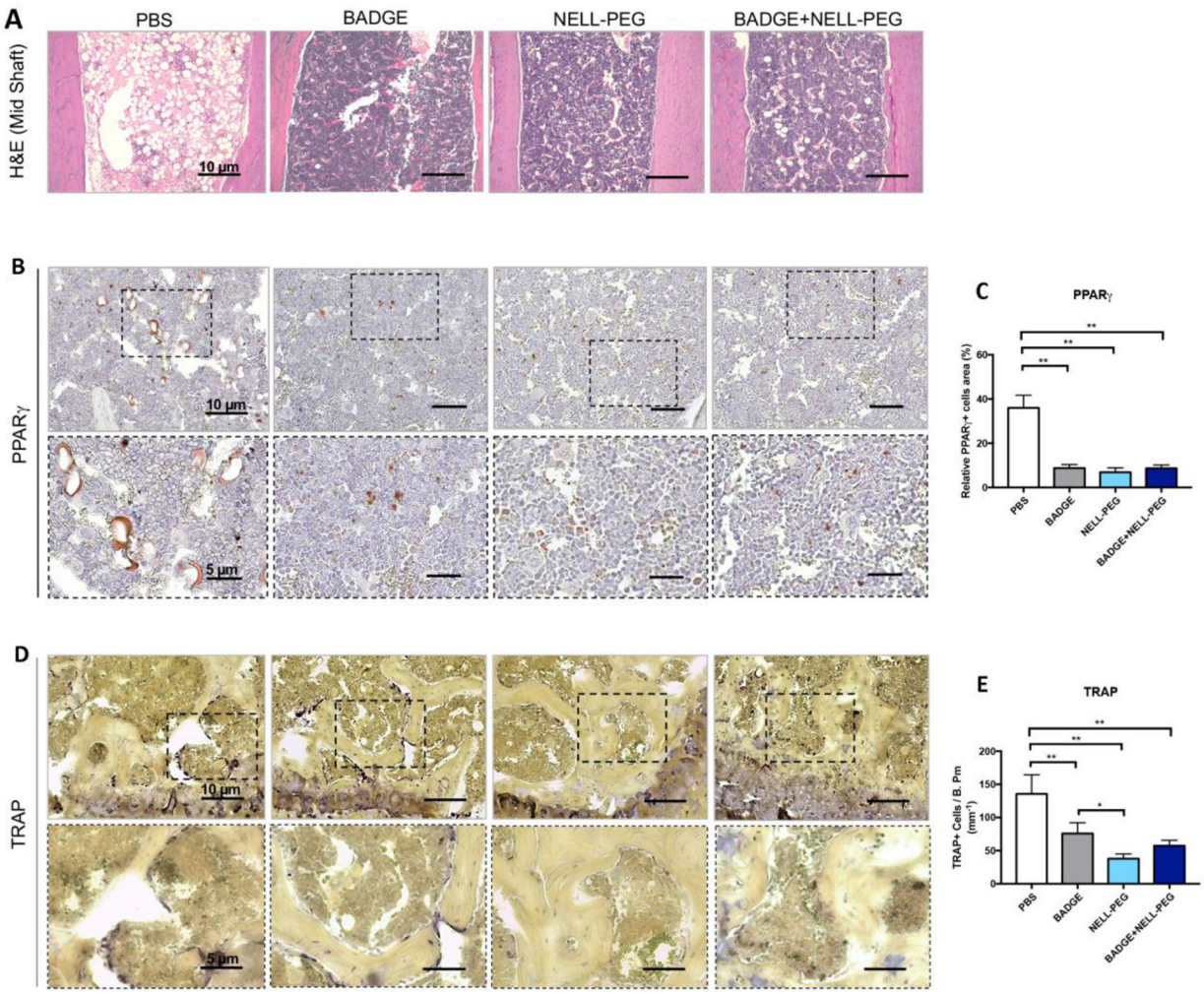

Figure 4. Histological and immunochemical analyses of bone marrow adipose formation and bone resorption in senile osteopenic mice.

(4A) H&E staining at the midshaft of the femur to examine bone marrow adipose formation. (4B-C) Immunohistochemical staining of PPARγ expression and analysis. (4D-E) TRAP immunohistochemistry and quantification of TRAP+ stained cells at the distal shaft of the femur. Data are presented as mean ± SD. *p<0.05, **p<0.01.

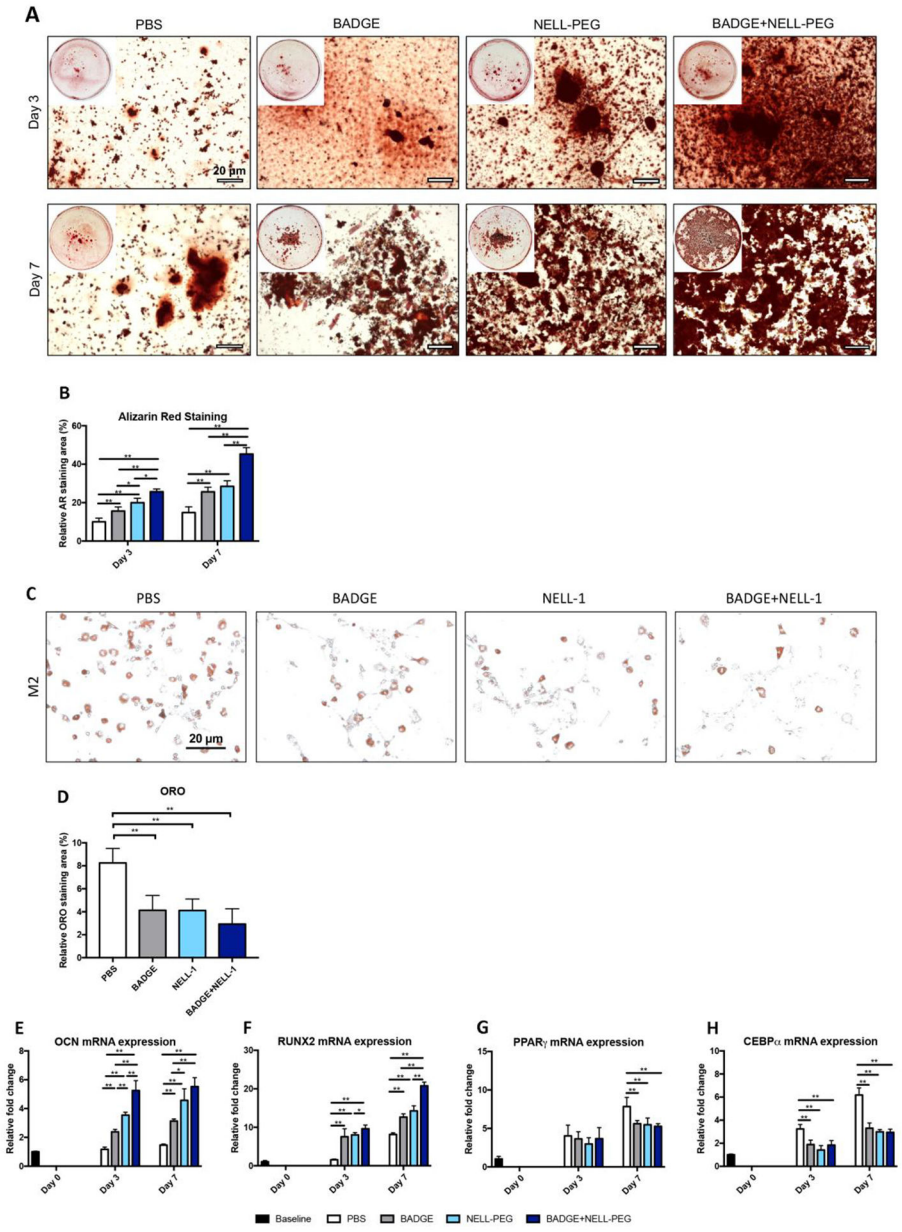

Figure 5. Effects of PPARγ suppression + NELL-PEG co-treatment on BMSC and M2 cells mineralization and adipogenesis.

(5A) BMSCs were isolated from senile osteopenic mice on day 3 and 7 post-injection. (5B) Quantification of Alizarin Red mineralization staining after BMSCs were isolated and cultured in growth medium for 3 days. (5C) M2–10B4 cells Oil Red O lipid accumulation staining after 14 days of adipogenic induction. (5D) Quantification of relative Oil Red O-positive staining area compared to the total cell area. (5E-H) RT-PCR quantification of OCN, RUNX2, PPARγ, and CEBPα from senile osteopenic mouse BMSCs isolated at baseline (day 0), day 3, and day 7 post-injection. Data are presented as mean ± SD. *p<0.05, **p<0.01.

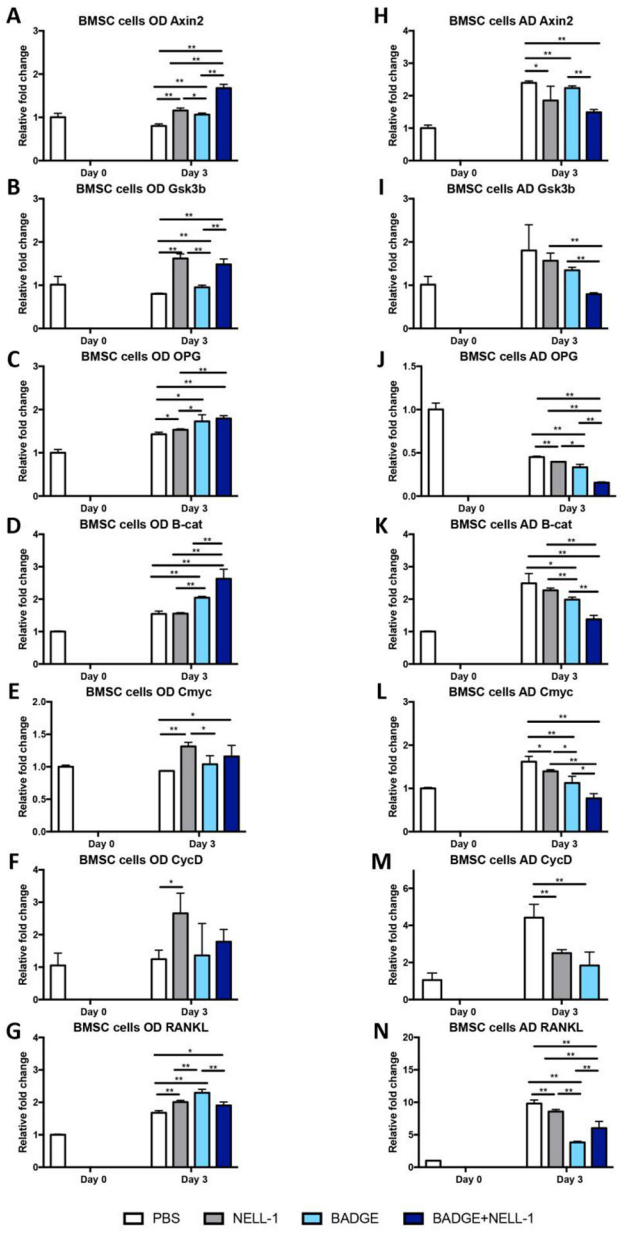

Figure 6. Effects of dual BADGE and NELL-1 treatment on gene expressions involved in the Wnt/β-catenin signaling pathway.

(6A-G) RT-PCR quantification of Axin2, GSK3b, OPG, β-catenin, Cmyc, CycD, and RANKL from senile osteopenic mouse BMSCs isolated at baseline (day 0) and incubated with osteogenic medium for 3 days. (6H-N) RT-PCR quantification of Axin2, GSK3b, OPG, β-catenin, Cmyc, CycD, and RANKL from senile osteopenic mouse BMSCs isolated at baseline (day 0), and incubated with adipogenic medium for 3 days. Data are presented as mean ± SD. *p<0.05, **p<0.01.

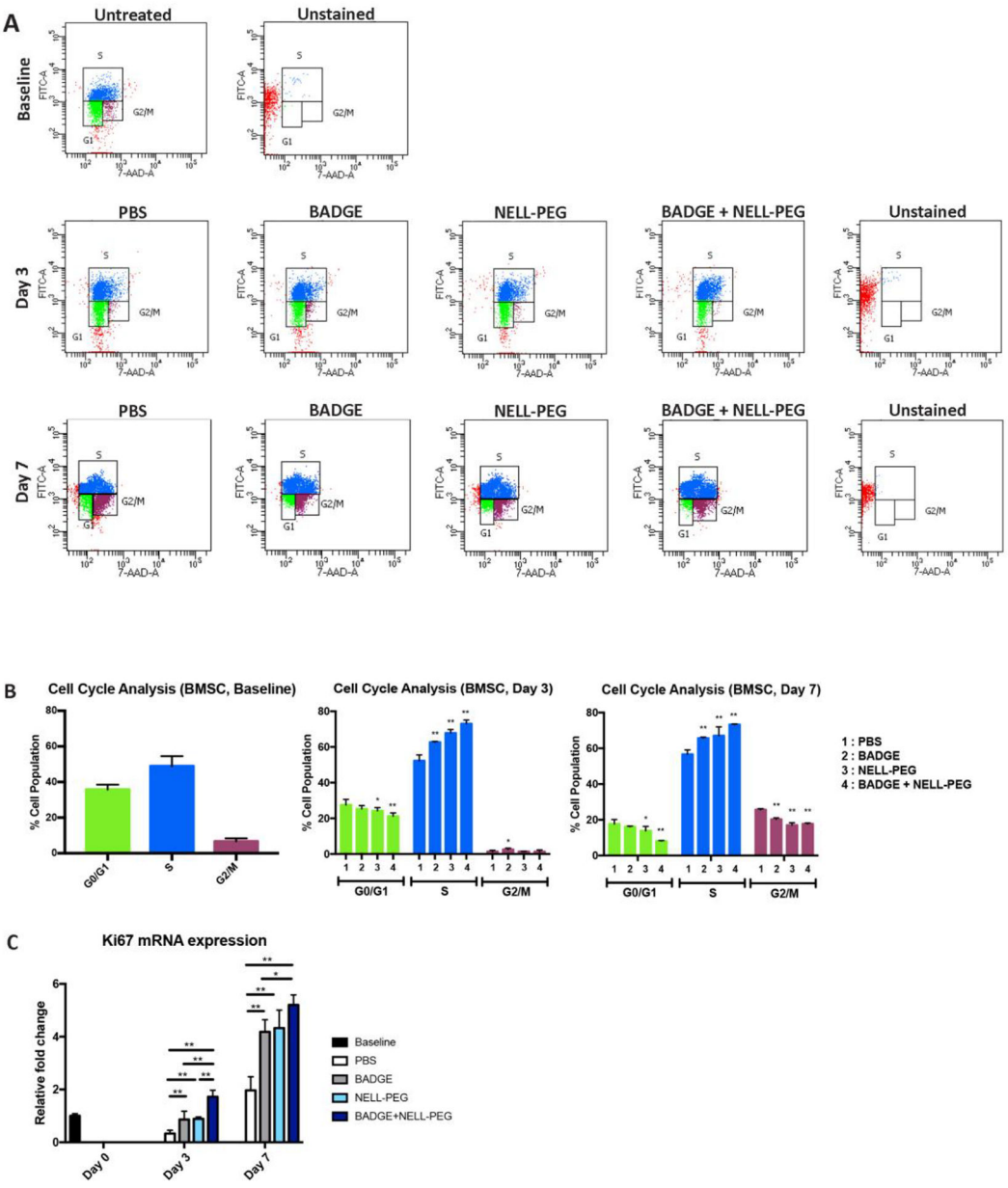

Figure 7. Cell cycle analysis of freshly isolated senile osteopenic mice BMSCs.

(7A) The 7-AAD plot and cell cycle distribution analysis of senile osteopenic mice BMSCs isolated on baseline (day 0), day 3, and day 7 post-injection. (7B) Quantification of cell population percentage in the G0/G1, S, and G2/M phases. Data are presented as mean ± SD. *p<0.05, **p<0.01. (7C) RT-PCR quantification of Ki67 mRNA levels in senile osteopenic mice BMSCs isolated on baseline (day 0), day 3, and day 7 post-injection. Data are presented as mean ± SD. *p<0.05, **p<0.01.

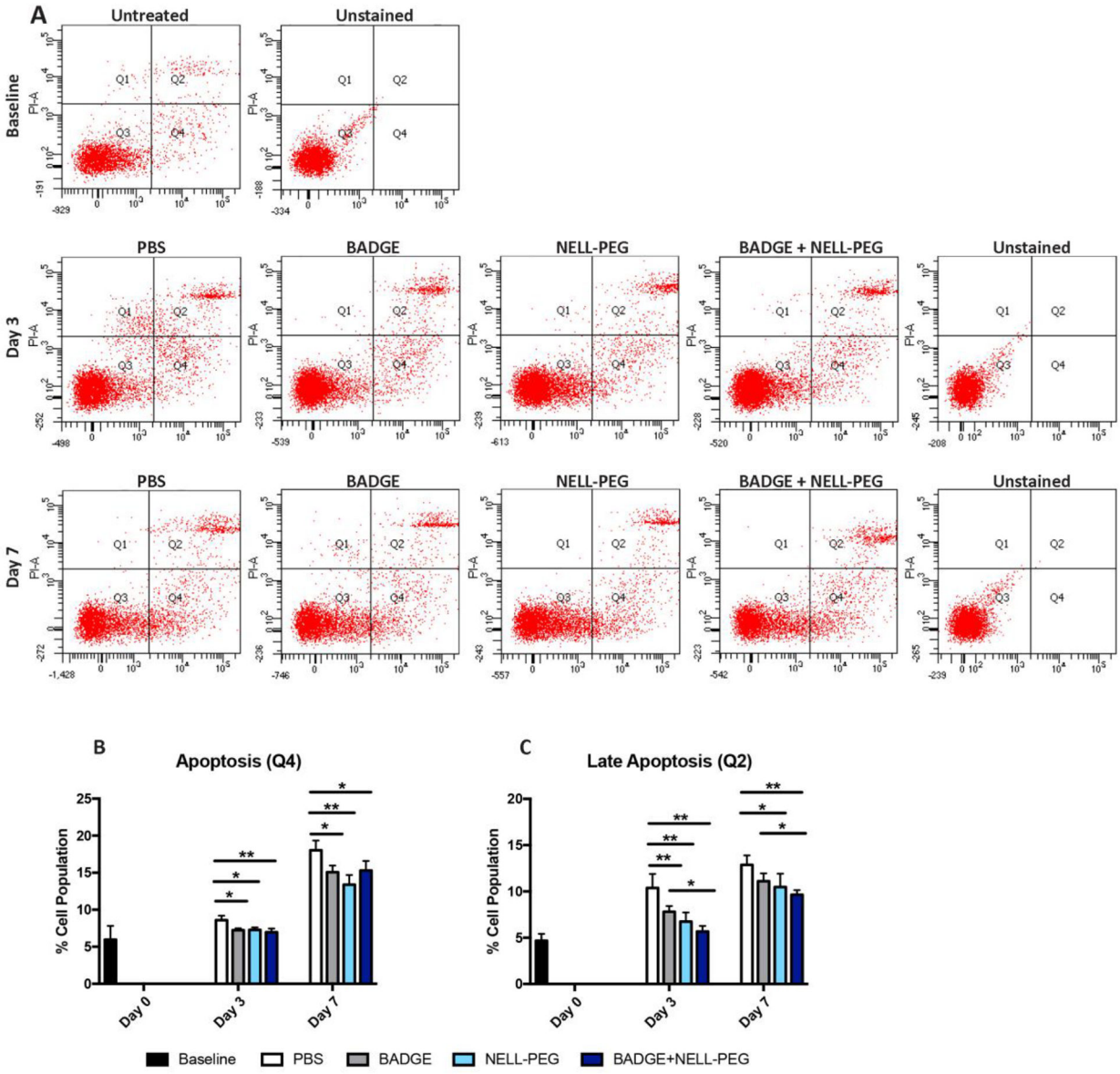

Figure 8. Apoptosis assay of freshly isolated senile osteopenic mice BMSCs.

(8A) Annexin V-PI plot of senile osteopenic mice BMSCs isolated on baseline (day 0), day 3, and day 7 post-injection. (8B-C) Quantification of cell population percentage in the early apoptosis (Q4) and late apoptosis quadrants (Q2). Data are presented as mean ± SD. *p<0.05, **p<0.01.